Science Concept 1: The Bombardment History of the Inner Solar System is Uniquely Revealed on the Moon

Science Concept 1: The bombardment history of the inner solar system is uniquely revealed on the Moon

Science Goals:

a. Test the cataclysm hypothesis by determining the spacing in time of the creation of lunar basins.

b. Anchor the early Earth-Moon impact flux curve by determining the age of the oldest lunar basin (South Pole-Aitken Basin).

c. Establish a precise absolute chronology.

d. Assess the recent impact flux.

e. Study the role of secondary impact craters on crater counts.

INTRODUCTION

The highest science priorities in the NRC (2007) report involved the impact cratering history of the Moon, in part because it had a dramatic effect on the Earth-Moon system and also because it forms the chronological timeline for processes that affected the entire solar system.

The Apollo program provided the first glimpse of that bombardment history. It revealed portions of the Moon that were quite ancient and nearly the same age as the solar system. The astronauts also recovered a large number of rocks that were involved in impact events in a narrow window of time, approximately 3.8 to 4.0 billion years ago, in an event that was described as a terminal impact cataclysm.

Those data indicated the Moon (and presumably the Earth and other terrestrial planets, including Mars) suffered an early, but extended period of bombardment. We are, however, still working in a data poor environment. That magnitude of that bombardment and the duration of potentially short interval events, such as the suspected event 3.8–4.0 Ga, remain uncertain. To evaluate models of that epoch, ages of some of the Moon's immense impact basins are needed, including that of the South Pole-Aitken basin, which is the oldest and largest recognizable impact basin on the Moon.

The Moon provides the best record in the solar system of the collisional evolution after the basin-forming epoch. Thus, suitable samples from a representative set of younger impact craters are also needed to resolve several outstanding scientific questions. If done well, those ages can provide a calibrated impact cratering chronology that can be applied to the other terrestrial planets.

In the following pages, each of the Science Goals within Science Concept 1 will be explored in additional detail. After that foundation has been established, a series of landing site criteria will be explored so that suitable locations for future missions can be identified.

SCIENCE GOAL 1A: TEST THE CATACLYSM HYPOTHESIS BY DETERMINING THE SPACING IN TIME OF THE CREATION OF LUNAR BASINS

Introduction

To test the cataclysm hypothesis, the temporal spacing and ages of the large impact basins on the Moon must be determined. The essential questions to be addressed are:

- What is the age of the oldest and youngest impact basins on the Moon?
- How are the absolute ages of the old impact basins distributed in early lunar history (continuous post-accretion decay of impact rate vs. sharp late heavy bombardment event)?

Crater counting dating methods widely used on the Moon can only be used to determine the relative age of the surface only and is subject to large uncertainty. To determine the precise age of a basin, laboratory radioisotope dating of rock samples produced by the impact (*i.e.* impact melt or impact melt breccia) must be performed.

Thus far, 43 large impact basins on the Moon have been identified (Spudis *et al.*, 1994; Spudis, 1993; Wilhelms, 1987; Fig. 1.1 and Table 1.1). Debate continues (Bryne 2008) regarding the existence of an ancient near side megabasin. The returned lunar samples (by Apollo and Luna programs) were subject to radioisotope dating, but are not representative for the whole lunar surface. Many of them might be part of perturbated megaregolith formed by ejecta of large impact basins (Petro and Pieters, 2008; Haskin, 1998; Haskin *et al.*, 1998; Head *et al.*,1993, Howard *et al.*, 1974; Moore *et al.*, 1974) and cannot be reliably attributed to a specific impact event (Korotev *et al.*, 2002).

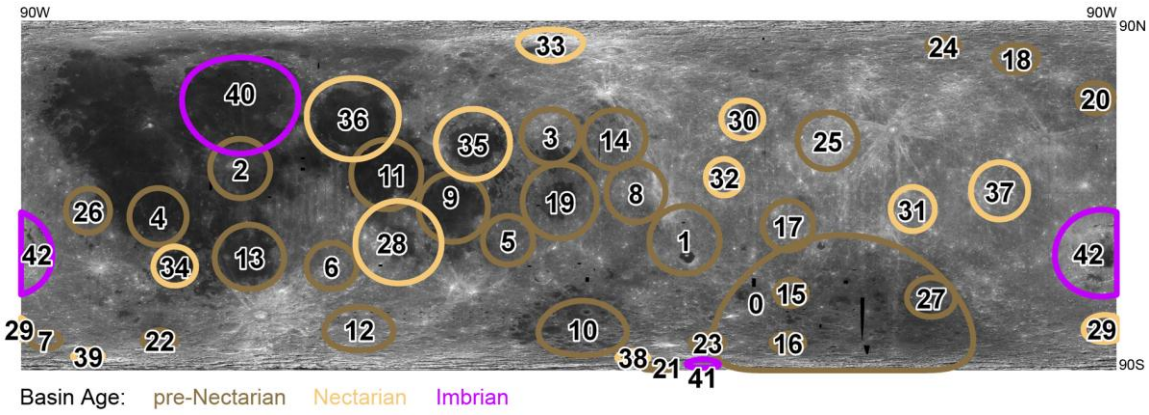

FIGURE 1.1 Forty three large impact basins identified on the Moon by Wilhelms *et al.*, 1987. The numbers correspond to the basin numbers listed in Table 1.1.

TABLE 1.1 Forty three large impact basins identified on the Moon by Wilhelms *et al.* (1987)

Number	Basin	Age	Lat. (°)	Long (°)	Main topographic rim diameter (km)	Transient cavity diameter (km)
0	South Pole-Aitken	pre-Nec	-56	180	2600	2099
1	Tsiolkovsky-Stark	pre-Nec	-15	128	700	409
2	Insularum	pre-Nec	9	-18	600	330
3	Marginis	pre-Nec	20	84	580	315
4	Flamsteed-Billy	pre-Nec	-7	-45	570	307
5	Balmer	pre-Nec	-15	70	500	252
6	Werner-Airy	pre-Nec	-24	12	500	252
7	Pingre-Hausen	pre-Nec	-56	-82	300	95
8	Al-Khwarizmi-King	pre-Nec	1	112	590	322

9	Fecunditatis	pre-Nec	-4	52	690	401
10	Australe	pre-Nec	-51.5	94.5	880	550
11	Tranquillitatis	pre-Nec	7	30	700	409
12	Mutus-Vlacq	pre-Nec	-51	21	690	401
13	Nubium	pre-Nec	-21	-15	690	401
14	Lomonosov-Fleming	pre-Nec	19	105	620	346
15	Ingenii	pre-Nec	-34	163	315	107
16	Poincare	pre-Nec	-57.5	162	325	115
17	Keeler-Heaviside	pre-Nec	-10	162	500	252
18	Coulomb-Sarton	pre-Nec	52	-123	440	205
19	Smythii	pre-Nec	-2	87	740	443
20	Lorentz	pre-Nec	34	-97	365	146
21	Amundsen-Ganswindt	pre-Nec	-81	120	335	122
22	Schiller-Zucchius	pre-Nec	-56	-44.5	335	122
23	Planck	pre-Nec	-57.5	135.5	325	115
24	Birkhoff	pre-Nec	59	-147	325	115
25	Freundlich-Sharonov	pre-Nec	18.5	175	600	330
26	Grimaldi	pre-Nec	-5	-68	440	198
27	Apollo	pre-Nec	-36	-151	480	236
28	Nectaris	Nec	-16	34	860	414
29	Mendel-Rydberg	Nec	-50	-94	420	281
30	Moscoviense	Nec	26	147	420	189
31	Korolev	Nec	-4.5	-157	440	205
32	Mendeleev	Nec	6	141	365	146
33	Humboldtianum	Nec	61	84	650	331
34	Humorum	Nec	-24	-39.5	425	358
35	Crisium	Nec	17.5	58.5	740	487
36	Serenitatis	Nec	27	19	920	657
37	Hertzsprung	Nec	1.5	-128.5	570	307
38	Sikorsky-Rittenhouse	Nec	-68	111	310	103
39	Bailly	Nec	-67	-68	300	95
40	Imbrium	Imb	33	-18	1160	744
41	Schrodinger	Imb	-75	134	320	111
42	Orientale	Imb	-20	-95	930	397

In the Apollo era, landing site selection was restricted to the near side and low latitudes. One of the goals of the Constellation program was to enable Moon-wide landing without such restrictions and it can be expected that future architectures will advocate a similar goal. Thus, there is an opportunity to select a globally-distributed set of landing sites based on scientific priorities.

Methodology and Requirements

Current technology does not enable robotic in-situ dating of lunar samples with the precision required. Samples from selected sites must be collected and returned to Earth in order to date precisely the beginning and development of early lunar impact basin formation and to reveal whether these were formed during a putative cataclysmic bombardment period.

In order to maximize the probability of successful sampling, the selected sites should fulfill the following criteria:

1. The locality has to provide solid confidence that the samples collected are directly linked to a specific impact basin
2. The samples have to be exposed and easily accessible
3. The samples have to be easily identifiable

Three terrains of impact basins potentially fulfill those criteria:

1. Proximal ejecta blanket containing impact melt breccia fragments
2. Impact melt sheet filling the interior of the basin
3. Modification zones of a basin with deposits of the impact melt or melt ponds splashed on the walls

Terrain selection

Terrain selection is determined primarily by the relative age of the basin and distance to other basins of younger age. In general, young basins have well exposed rims, inner rings, and proximate ejecta composed of melt breccia enabling relatively easy sampling. In contrast, rim structures and ejecta of old basins are eroded and covered by superposed ejecta of younger basins (forming a magaregolith layer). In these cases the central melt sheet may provide the most reliable source of sampling material. The central melt sheet is often buried under regolith as well and in most cases it is additionally covered by mare basaltic flows. However, as will be outlined below, young impact events of sufficient size may penetrate the regolith and mare basalt layers and expose the underlying melt sheet for sampling.

As an example, two impact basins (Mendel-Rydberg and Schrödinger) and the corresponding best terrain evaluation is outlined in Table 1.2.

TABLE 1.2 Terrain evaluation for Mendel-Rydberg (old) and Schrödinger (young) impact basins.

Basin name	Age	Appearance	Perspective terrains
Mendel-Rydberg	pre-Nectarian, estimated to be formed just after SPA	Topographic features highly eroded and buried by younger ejecta depositions.	Central melt sheet might be still preserved. However the thickness of megaregolith and mare fill has to be precisely evaluated in order to estimate the depth of melt sheet. Young small craters penetrating to desired depth excavate melt sheet material for sampling.
Schrödinger	Lower Imbrian	After Orientale the youngest impact basin with well exposed rim structures and ejecta.	Basin floor, melt breccia and melt ponds on rim structures, or alternatively the proximate ejecta.

Proximate ejecta blanket containing impact melt breccia fragments

During a basin-forming impact part of the generated melt is excavated and launched from the crater with other ejecta. The ejected material forms a continuous proximal ejecta blanket near the basin and a discontinuous distant ejecta blanket at larger distances. Large impact events may produce global ejecta

reaching even the antipode, forming antipodal enriched deposits. Here, the ejecta meets and forms a local maximum in its thickness (Moore *et al.*, 1974).

The cumulative ejecta thickness of 42 largest lunar impact basins has been modeled by Petro and Pieters, 2008 (Fig. 1.2). The results indicate the cumulative ejecta thickness to be on average 500–1000 meters on the near side and 100–500 meters on the far side.

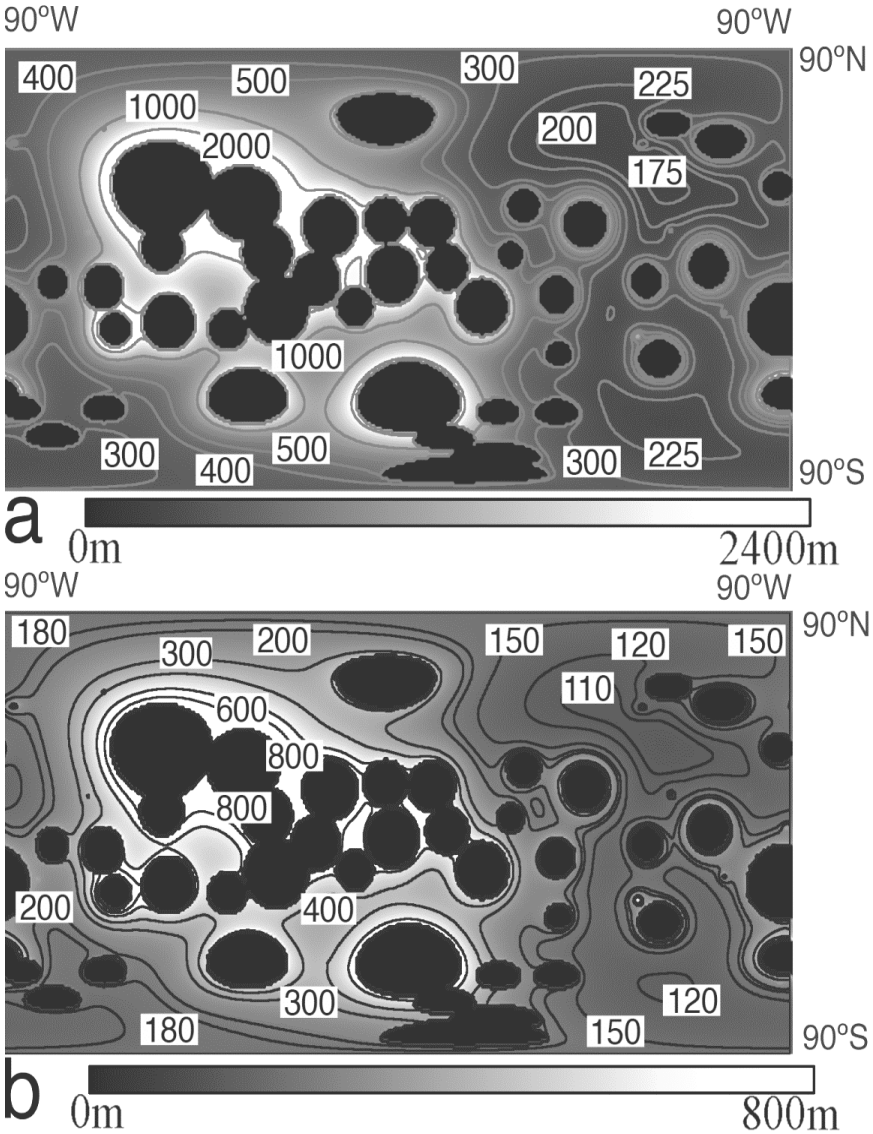

FIGURE 1.2 Lunar-wide cumulative amount of ejecta from 42 lunar basins as listed in Table 1.1 (South Pole-Aitken basin is not included in this figure) estimated utilizing the ejecta equations of (a) Pike (1974) and (b) Housen *et al.* (1983). The area inside of the main topographic ring for each of the 42 basins is filled in black. Adapted from Petro and Pieters, 2008.

Distant ejecta impacts the surface at high speeds causing significant erosion and mixing with the surface material during its deposition. Due to this fact it is not reliable to search for melt fragments in distant ejecta because the melt is mixed with regolith or older ejecta deposited by preceding impact events. According to calculations by Petro and Pieters (2008), most of the lunar surface might be mixed to depths of order 10–100 m (Figs. 1.3 and 1.4).

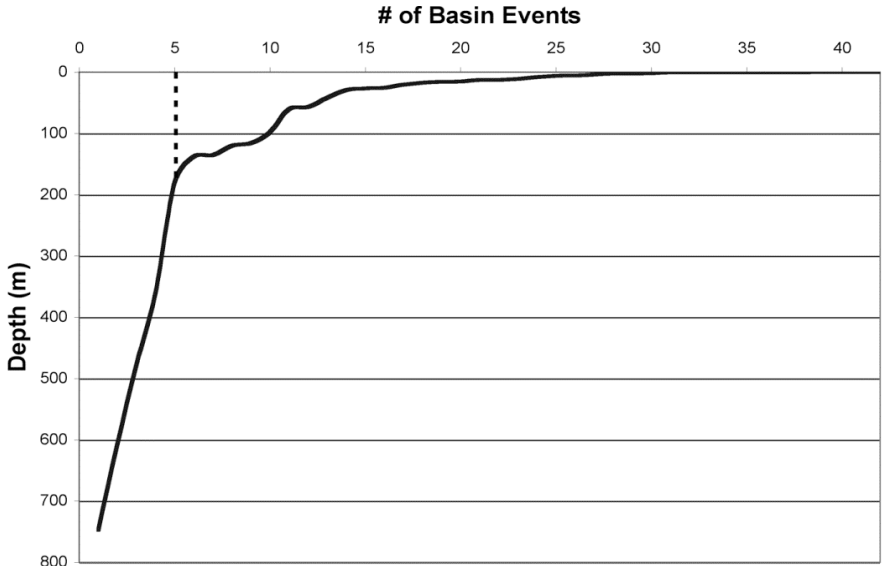

FIGURE 1.3 Depth mixed by each of the 42 basin events listed in Table 1.1 (South Pole-Aitken basin is not included in this figure) at the Apollo 16 landing site. The depth mixed by 5 events is marked with a dashed line. The five deepest mixing events are, from deepest to shallowest: Serenitatis, Imbrium, Tranquillitatis, Nubium, and Crisium. Adapted from Petro and Pieters, 2008.

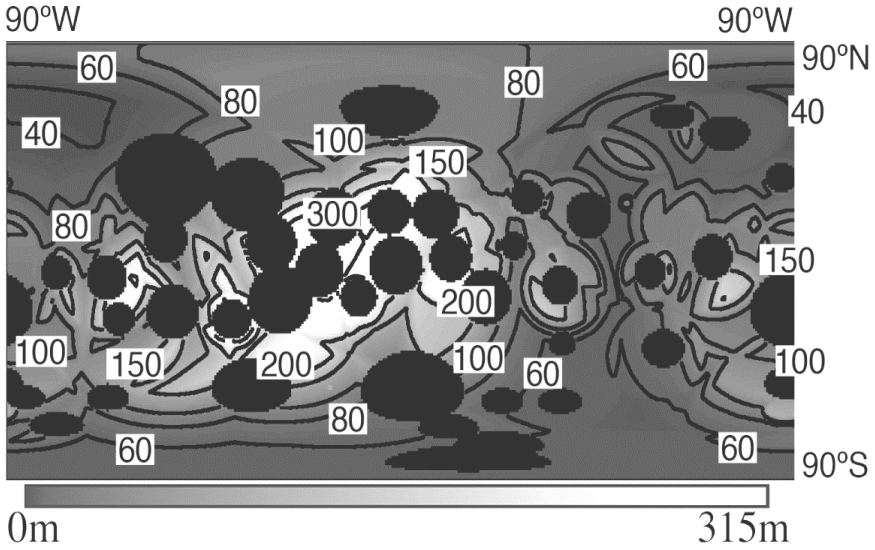

FIGURE 1.4 Depth of megaregolith mixed by at least five basin events as estimated utilizing the Housen *et al.* (1983) ejecta model and a μ/2 mixing ratio. The area inside the main topographic ring for the 42 basins is filled in black. Adapted from Petro and Pieters, 2008.

Only well-exposed proximal ejecta of young impact basins (like Imbrium, Orientale, and Schrödinger) can provide exposed and easily accessible representative material containing melt fragments suitable for sampling. Ejecta distribution modeling and surface distribution and thickness measurements of Imbrium and Orientale ejecta are summarized in Haskin *et al.* (1998; Imbrium), Ghent *et al.* (2008; Orientale), Moore *et al.* (1974; Orientale), and Head *et al.* (1993; both basins).

Impact melt sheet filling the interior of the basin

Samples obtained directly from an impact melt sheet have several advantages. The location of the impact melt sheet within a basin provides strong confidence that a sample is related to the desired impact event. The slow cooling rates of massive melt sheets provide sufficient time for melt degassing important for reliable radioisotope dating. Impact melt within large basins should contain no or little brecciated fragments of the target rock resulting in the highest melt-to-bulk sample gain.

However, several difficulties exist and have to be overcome in order to obtain a desired melt sheet sample. Melt sheets may be covered with impact melt breccias which may or may not provide an equally reliable sample suitable for radiometric dating. Most of the large impact basins experienced subsequent basaltic mare flooding, covering the central melt sheet. Additionally, the surface of impact basins might be covered and disturbed by impact ejecta from younger impact events. The thickness of overlying impact ejecta increases with the age of the impact basin and most of the old pre-Nectarian and Nectarian basins seem to be completely buried and reworked by subsequent deposition of younger ejecta layers.

The thickness of mare fill and overlying ejecta is poorly known. Precise knowledge of these factors is essential in determining the depth of the melt sheet layer. In the past, estimates of crater fills was based on partially flooded crater morphology studies. Additionally, radar sounding measurements during the Apollo 17 mission successfully determining the vertical structure of several impact basins and maria. The results indicate the thickness of mare fill (including the regolith layer) to be typically a few tenths of meters to a few kilometers (Jolliff *et al.*, 2006) and are summarized in Table 1.3.

TABLE 1.3 Basalt thickness estimates in large impact basins (compiled from Jolliff *et al.*, 2006).

Basin	Age	Thickness (km) from flooded crater morphology (Williams and Zuber, 1998)	Thickness (km) from Apollo 17 radar sounding
Smythii	Pre-Nec	1.3	
Grimaldi	Pre-Nec	3.5	
Nectaris	Nec	0.8	
Humorum	Nec	3.6	
Crisium	Nec	2.9	1.4
Serenitatis	Nec	4.3	0.9–1.6
Imbrium	Imb	5.2	
Orientale	Imb	0.6	
Proccelarium	Pre-Nec	1	0.6–1

There is, however, considerable spatial variability in mare thickness due to the uneven nature of the basin floor and the possibility of multiple mare flows. Several methods are or could be available to improve knowledge of the basin subsurface structure and determine the thickness of mare flows and overlying megaregolith, including orbital radar/radio sounding (*e.g.*, the LRS [Lunar Radio Sounding] instrument aboard Kaguya) and robotic or human-operated shallow refraction seismic surveys in selected areas.

The thickness of the impact melt sheet itself is also an important measurement to make. Estimates based on melt volume calculations usually predict a few-km-thick layer in the central area of the basin thinning towards the rim. Methodologies would be the same as outlined above.

Knowledge of impact basin subsurface structure is essential for melt sheet sampling. Once the location, depth, and thickness of the melt sheet are determined, the most promising sampling sites can be searched. Young impact craters superimposed on the basin melt sheet can excavate subsurface layers. The Lunar Impact Crater Database (Losiak *et al.*, 2009; Ohman 2011) is a valuable resource in searching for suitably large craters excavating the central melt sheet of large impact basins.

Fragments of the impact melt or melt ponds splashed on the walls of basin rims

During the impact process the melt is not only deposited in the form of central melt sheet, but also trapped in the form of melt ponds or impact melt breccia on the inner walls of the basin, inner rings, or central peak structures (Fig. 1.5). In such places the melt is relatively exposed readily accessible, although the rim/ring and central peak structures represent areas with potentially difficult topography (*e.g.*, steep and possibly unstable slopes, ~km elevation differences, etc.), thus increasing safety risk and engineering challenge.

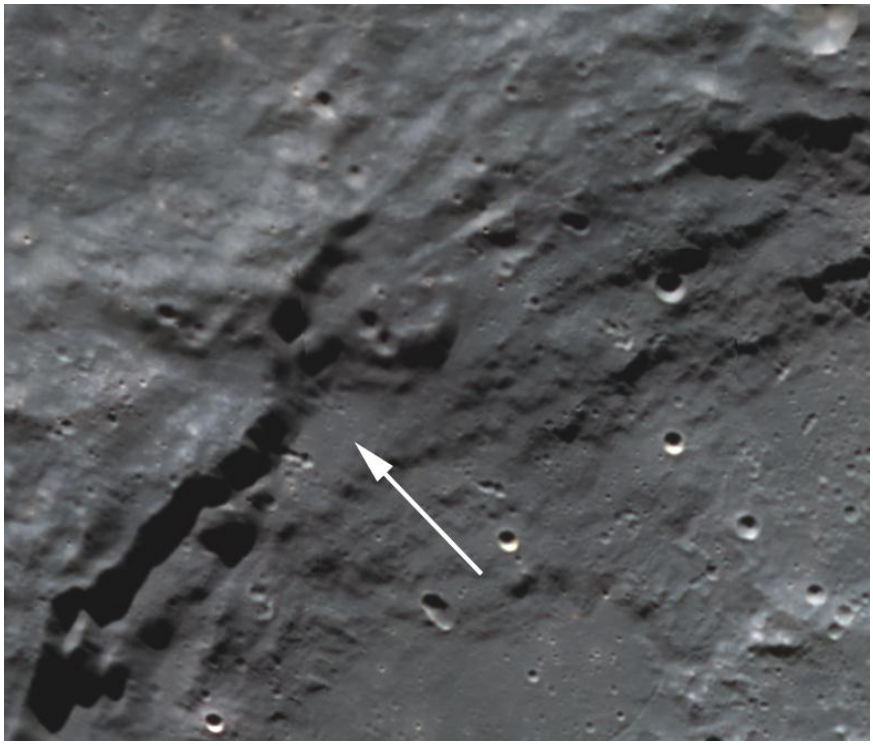

FIGURE 1.5 Potential melt pond on the NW rim of Schrödinger basin.

Conclusions

While the proximal ejecta blanket containing impact melt breccia fragments and deposits of the impact melt or melt ponds splashed on the walls are suitable collection sites for relatively young, well preserved, and well exposed impact basins, sampling impact melt sheets filling basin interiors, despite being the most challenging method, is probably the only option to collect and date the melt of old significantly eroded and buried basins. Even if the central melt sheet is covered by younger units, fresh smaller impact craters may excavate the surface to specific depth where the central melt sheet is buried and expose it for sampling.

SCIENCE GOAL 1B: ANCHOR THE EARLY EARTH-MOON IMPACT FLUX CURVE BY DETERMINING THE AGE OF THE OLDEST LUNAR BASIN (SOUTH POLE-AITKEN BASIN)

Introduction

In order to determine the age of the South Pole-Aitken basin (SPA), material created or affected by the SPA event needs to be located, sampled, and returned to Earth for radiometric dating. This material may be in the form of impact melt or a melt breccia, and may be mixed with regolith. Such materials need to be identified and in some cases higher resolution orbital imagery will be needed to do so. Examples of type localities for SPA impact-related material are presented here, but this list is by no means encompassing.

Background

The SPA basin extends roughly from the South Pole to Aitken crater on the lunar far side. Centered upon 56° S, 180°, with a diameter of about 2600 km (Spudis *et al.* 1994), and on average 12 km deep (~1.5 times taller than Mt. Everest), it is the largest known basin on the Moon (Fig. 1.6). The formation of large basins is still largely not well understood (as the SPA basin has no representative analog on Earth), and better understanding of such processes will come with missions to basins like SPA.

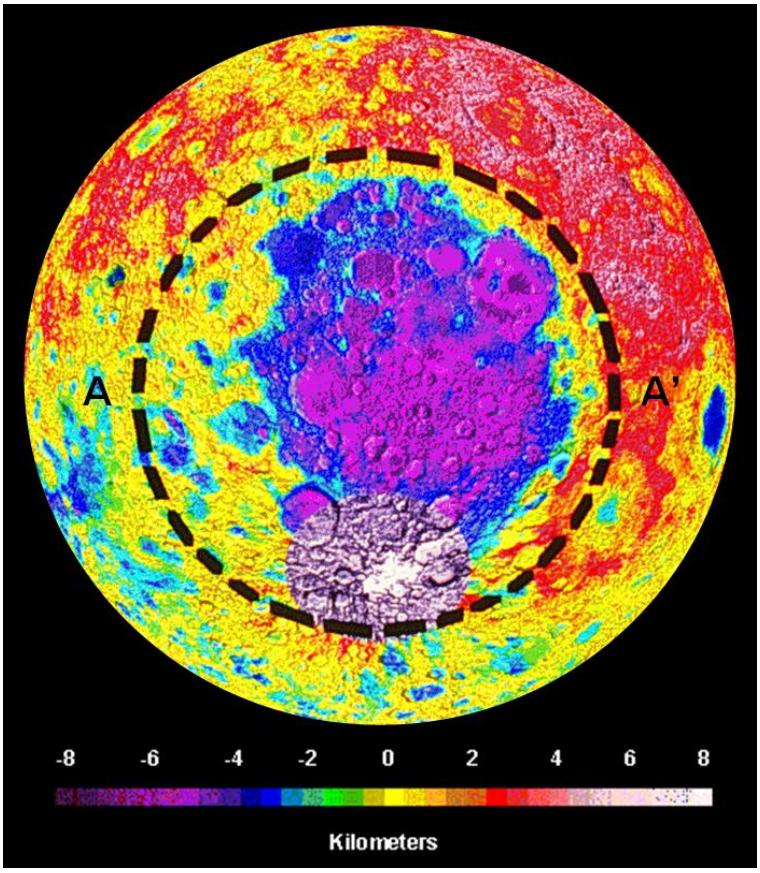

FIGURE 1.6 Clementine topographic image centered on the center of SPA basin. Dashed line indicates interpreted main rim of the basin. Gray areas indicate no data. Image courtesy of NASA.

Hartman and Kuiper first speculated on the presence of a large basin on the far side of the Moon in 1962 when a large mountain range was observed on the near side of the moon near the South Pole. This mountain range stands 8–9 km high, and is called the Leibniz Mountains (Hartman and Kuiper 1962). Apollo era instruments also detected an anomaly on the far side, but it was not until Clementine imagery that the existence of a large basin was confirmed.

Hiesinger and Head (2003) identified three SPA rings (and possibly four) based on Clementine altimetry data. Each of the rings is marked by a 2–4 km drop in elevation, and they are best identified in the northeastern parts of the basin (Hiesinger and Head 2003). The Leibniz Mountains lie on the main topographic ring of the SPA basin.

Since the SPA impact event, the basin has been subjected to billions of years of impact degradation, thus making the identification of peak rings, melt sheets, and impact ejecta difficult to impossible to identify. Although SPA is old, it has had surprisingly little modification due to volcanism, unlike the Mare-filled Procellerum terrain. Volcanic deposits occur mostly within craters and basins, and are upper Imbrian to Eratosthenian in age (Wilhelms, 1979). SPA is home to multiple large basins, including Apollo, Mendel-Rydberg, Planck, Poincare, and Schrödinger, ranging from the Pre-Nectarian to Erathoseinan in age.

The topography surrounding SPA basin is not uniform, and some authors have attributed this to a low angle oblique impact (Schulz, 1997). This non-uniformity may also be due to pre-existing topography created from large-scale impacts (Hiesinger and Head 2003). Whatever the reason, the surrounding plains are on average 6 km higher in the northeast quarter. Hiesinger and Head (2003) also outlined a possible pre-SPA basin ring that occurs within the main ring of SPA. These structures are incredibly hard to identify with any accuracy, but higher resolution imagery will make this an easier task.

Based on the number of ring structures and the extent to which they are slumped, it is believed that the SPA impact event took place in a sufficiently non-viscous media (*e.g.*, Heisinger and Head 2003, Spudis *et al.* 2008), *i.e.*, after the crust and mantle had cooled to some extent.

Establishing an absolute age for SPA will set a critical point on the Impact Flux Curve, allow us to better understand the bombardment history of the Moon, and understand large scale basin formation processes.

Impact Melt

In general, impact melt can be found in a number of locations both within a basin and exterior to it. The highest concentration of impact melt will be found within the inner-most ring of SPA as a melt sheet, however the central melt sheet of SPA has been covered and reworked for billions of years. Identifying what is SPA melt versus what is melt from subsequent impacts may be possible with better imaging. There is the possibility that SPA melt does not occur at the surface of the basin, but rather as outcrops within the walls of deep basins overlaying SPA. SPA melt may also outcrop as the central peak ring of multi ring basins, like Schrödinger Basin. The central melt sheet will be differentiated to an unknown extent, and positive SPA identification may not occur until the sample is returned to the Earth.

Impact melt will also occur as a coating on the inner rings of the basin, though the nature and extent of this coating is not well described for large basins. Impact melt can also be found on the walls and rim of the basin, but due to the age of the basin, it is unlikely that an exact location for such sampling can be specified. Unlike smaller craters and basins, which have a veneer-like coating on the rim and walls, SPA will likely have both veneer and large massifs of pure melt occurring on the rim and walls. Identification of veneer is possible in young craters, and may possible for SPA with higher resolution imagery.

Identification of impact melt has some level of uncertainty, but Pieters *et al.* (2001) have identified areas of high Fe concentration near the center of the basin, termed Olivine Hill, which they take to be SPA melt material. Olivine Hill may also be uplifted upper mantle material, foreign deposits from a nearby basin or crater, or an olivine-rich cryptomare deposit (Pieters *et al.* 2001).

Impact melt may also be concentrated in pre-Nectarian age areas. Wilhelms (1987) identified Pre-Nectarian outcrops, as seen in Fig. 1.7. Pre-Nectarian age areas will have a higher concentration of SPA melt because they have not been covered with the ejecta of subsequent large basins and craters. Small, young craters in these areas will provide a fresh surface upon which to sample.

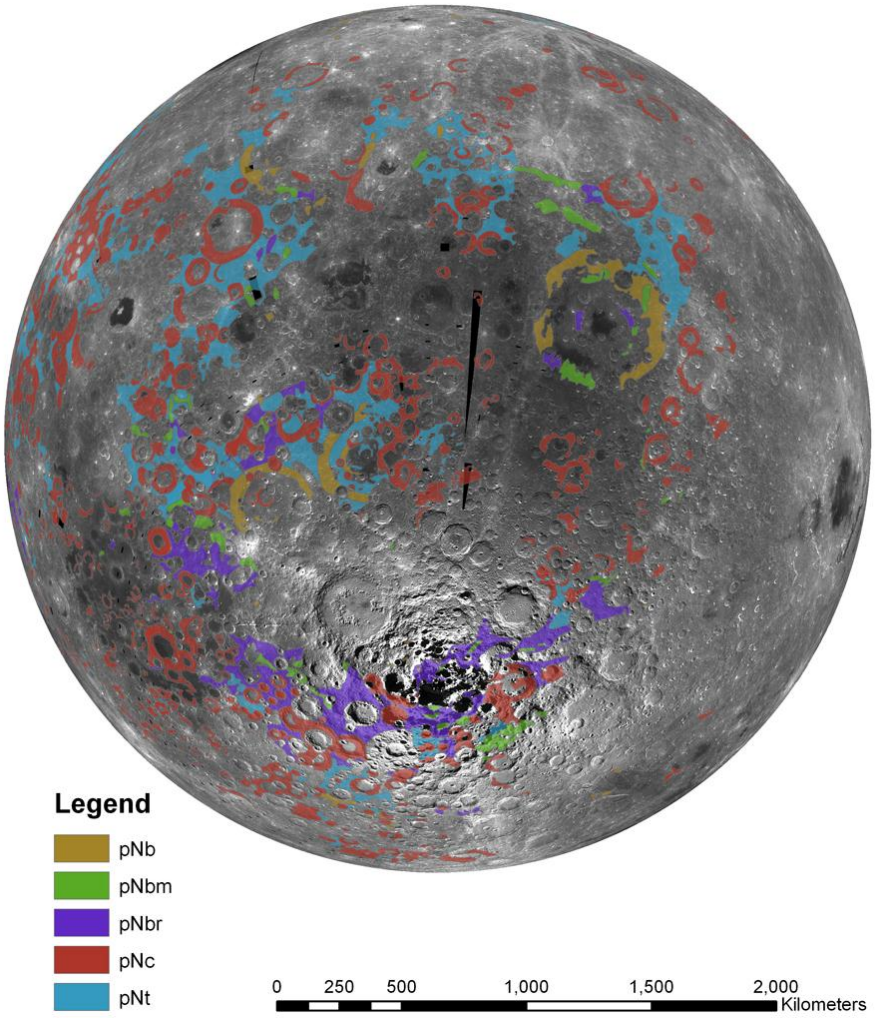

FIGURE 1.7 Pre-Nectarian aged outcrops, as identified by Wilhelms 1979. Image is centered on the center of SPA.

Impact Breccia

SPA impact breccia occurs as a layer within the basin, overlying the central melt sheet, but the depth of this breccia is not known. This impact breccia has also been subsequently overlain by debris from other basins, but like impact melt, it may possibly have a unique geochemical signature. It is not known if all of the impact breccia created by the SPA event would be melted enough to reset the age of the rock. However, the rock would still provide valuable insight into the processes that form impact breccias.

Impact Ejecta

Because the SPA impact penetrated so deep into the crust, it excavated rocks that are significantly different than those that occur on the surface, so SPA ejecta presumably have a unique geochemical signature. Petro and Peiters modeled the ejecta blanket of SPA, and determined thicknesses to be on the 1000's of meter scale (Fig. 1.8). Because of SPAs large size, impact ejecta can occur not only as massifs, but also as entire mountain ranges. One such range is the Leibniz Mountains, and occurs on the rim of SPA. Young, deep craters in the Leibniz may expose SPA affected material. Young craters are needed because they will not have been filled with thick ejecta from other impacts, and deep craters are desired because they would have the greatest possibility of excavating SPA melt material. One such crater that fits these criteria is Boussingualt. Although this crater has a small diameter, it is deep because a second

impactor hit the existing crater almost directly in the center. The result is a crater that is unusually deep for its diameter. The crater walls of Boussingualt would provide outcrops that are deep enough stratigraphically to sample SPA impact ejecta.

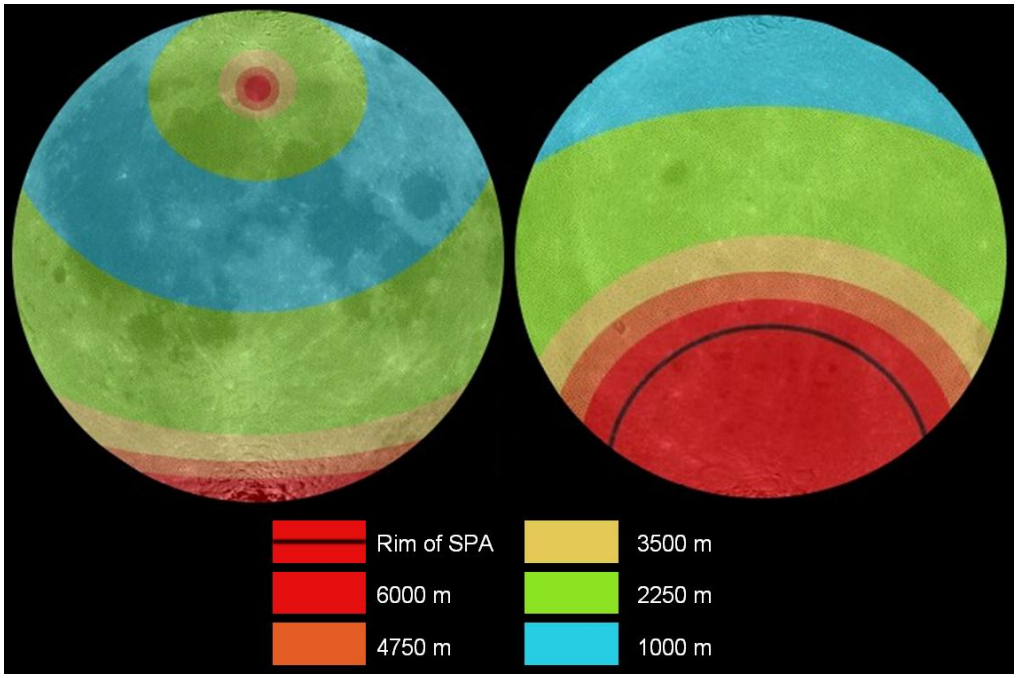

FIGURE 1.8 SPA ejecta thickness (after Petro and Peiters, 200X).

Massifs of melt can be identified as areas of rough terrain and high topography. Identifying these areas with better accuracy will be possible with higher resolution imagery. Craters within these massifs would provide outcrops to sample SPA material.

When impact ejecta is deposited, the layer directly beneath it becomes mixed. The nature of an SPA impact ejecta layer within the wall of a crater is not known; it may be semi-pristine or significantly gardened.

Regolith

Petro and Peiters (2004) estimated the regolith within SPA to contain 50–80% of SPA material, however, there are many assumptions associated with this model. If SPA material has a unique geochemical signature, it may be possible to locate chunks of it within the regolith, and if some areas have high concentrations of SPA material, it may be possible to detect them from orbit with high resolution imagery. Areas outside of SPA containing a significant portion of SPA melt need to be identified – layers of highest concentration will be stratigraphically lowest and will be affected by mixing.

Modeling Approaches

Even with limited data, some estimates of SPA excavation depth and the amount of SPA melt material present on the surface can be made. If the SPA event excavated the entire lunar crust and now outcrops upper mantle material, then SPA would be the only place on the Moon to easily sample mantle material. Using two different models, Petro and Pieters (2008) estimated ejecta from 42 lunar basins to be about 200–300 meters thick within SPA. Petro and Pieters (2004) attempted to determine the amount of SPA melt breccia still within the basin and estimated regolith to contain 50–80% of SPA material.

SCIENCE GOAL 1C: ESTABLISH A PRECISE ABSOLUTE CHRONOLOGY

Introduction

Basic lunar stratigraphic and chronologic relationships have been revealed based on inferred relative ages of surfaces from crater counting analyses of orbital images and absolute dating of returned samples. Ejecta deposits of impact craters and basins and mare basalt flows serve as chronostatigraphic 'marker horizons' that in turn allow the relative dating of other, inaccessible lunar surfaces (NRC 2007). Absolute ages of relatively few lunar chronostratigraphic units are known, however, and even some of those are uncertain. Apollo samples allowed dating of some mare surfaces as well as specific small craters (*e.g.*, North Ray), but significant uncertainties still remain for some craters important in defining chronostratigraphic units (Stöffler and Ryder, 2001), *e.g.*:

- Copernicus was dated based on rays sampled by Apollo 12 to be ~800–850 My old, but the identification of the dated samples as definitively Copernican ray material is uncertain and dating based on crater counts suggests that Copernicus may be as old as 1.5 Gy.
- Tycho's age was determined to be ~109 My old by dating the landslide (inferred to have been triggered by Tycho ejecta) that occurred near Apollo 17 landing site, as well as the "Central Cluster" craters that were proposed to be secondary craters of Tycho, but these associations are equivocal.
- Autolycus is a crater with visible rays (thus usually assumed to be Copernican in age) dated based on ray material sampled by Apollo 15 to be 2.1 Gyr old, and, thus, being part of Eratosthenian period. However, it is possible that the ray assigned to Autolycus was in fact formed by the Aristillus impact (Stöffler *et al.* 2006).

These three craters are the only relatively large craters that were dated during the Apollo era.

Similarly, ages of some mare surfaces have been established (samples from Apollo 17, Apollo 11, Apollo 15, Luna 16, Luna 24, Apollo 12). They cover a very restricted time period between (3.75 Gyr – Upper Imbrian, to 3.15 Gyr – Eratosthenian) (Stöffler *et al.* 2006). Other methods used to establish surface ages suggest that some of the maria visible on the surface of the Moon are much younger or older (*e.g.*, Heisinger *et al.* 2000, 2002, 2003). Determining the age of the entire range of mare basalts in an accurate way is necessary to reveal the duration and flux of lunar volcanism (Science Concept 5).

Lunar chronology

The most generally accepted lunar geologic chronology is the one established by Wilhelms (1987). This chronology divides lunar history into five main epochs: the pre-Nectarian (>3.92 Ga), the Nectarian (3.92 to 3.85 Ga), the Imbrian (3.85 to 3.2 Ga), the Eratosthenian (3.2 to 0.8 Ga), and the Copernican (<0.8 Ga) (Fig. 1.9). Only the lower Imbrian and earlier time boundaries are known with any accuracy, because of the Apollo and Luna samples. The later periods are based on relative stratigraphy of surface features and the boundaries are approximate.

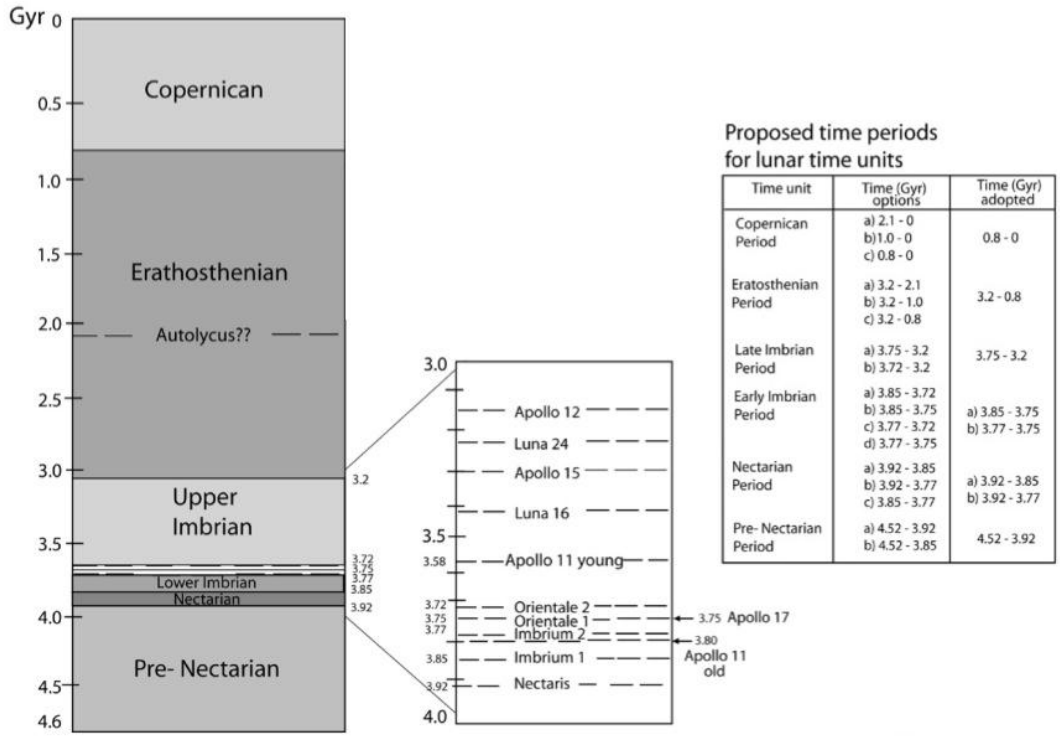

FIGURE 1.9 Lunar chronology and proposed and adopted time boundaries. The middle inset shows various radiometric ages from the Apollo and Luna samples. Note the very limited time range sampled by lunar missions. This explains the uncertainty on the time boundaries. Figure modified from Stöffler *et al.* (2006).

Lunar chronology is based on:

Superposition relationships

The superposition principle states that older units are overlaid by younger ones. Only the relative age of units can be revealed in this manner. Assuming that absolute ages of some 'marker' surfaces are known it is possible to establish semi-relative ages of other surfaces that are in contact with the markers. For example, knowing the age of Copernicus to be ~800 My and seeing that another surface feature is partially covered by Copernicus ejecta, it is possible to deduce that this other feature is older than 800 My. If marker surfaces cover large area, and are evenly distributed in time and space they could become a base for establishing the chronology of entire lunar surface.

Crater counting

The density of craters on a particular surface can be used to calculate the relative age of that region. The density of impact craters on the lunar surface generally increases as the surface ages increases. Craters are emplaced at random, with smaller impactors are more common than large ones. After some time a surface becomes saturated with craters, because there are so many impacts that they start to fall in the same place. Surfaces are first saturated with smaller craters (because small impactors are much more numerous) and later with larger ones. Because of saturation, crater counting must be done for craters larger than a specific saturation value, larger for older surfaces (*e.g.* for Lower Imbrian 500 m, while for Copernican it is only 10 m).

A major limitation of the crater counting method is that knowledge of the lunar impact flux is imprecise, and the curve is calibrated precisely only for the time span between about 3.8 and 3.2 Ga. Other time periods are often calibrated with use of single points (Fig. 1.10). Calibration of the curve is made based on the reference surface approach. A reference surface is an initially craterless surface (such as a mare basalt flow) that can be radiometrically dated that has had crater counting analysis performed on it. The extent of our lack of the knowledge about lunar impact flux is best illustrated by the fact that there is

still on-going debate about the extent and even occurrence of the Late Heavy Bombardment (LHB) (*e.g.*, Bogard, 1995; Cohen *et al.*, 2000).

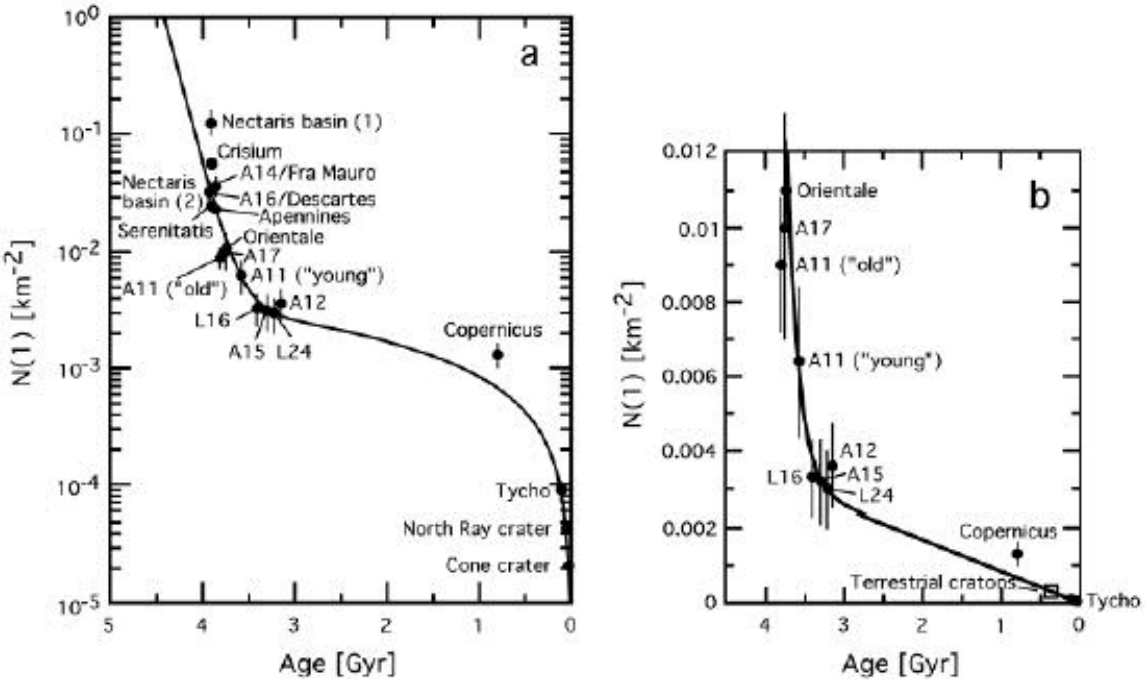

FIGURE 1.10 Cratering rate plot in log scale (a) and in linear scale (b). Error bars are large and some of the points are far off (Copernicus, Nectaris) from the production function. (Fig. 10 from Neukum *et al.* [2001])

Secondary craters created by the impact of primary crater ejecta back onto the surface can strongly but locally increase the number of craters visible on a surface (Shoemaker 1960). Some secondary craters are easily recognizable from their morphology, but others (especially those formed from the highest-speed and most distal primary ejecta) are not. The population of small craters used to date younger or small surfaces can be strongly influenced by secondaries.

The crater counting method is not appropriate for very small areas because the errors are too large. Crater counting is a statistical method and thus requires a sufficiently large number of craters for acceptable errors. Table 1.4 shows minimal areas of surfaces required for reliable application of the crater counting method.

TABLE 1.4 Minimal area (km^2) necessary for statistically satisfactory crater counting with respect to different minimal crater sizes, assumed percent error, and time.

For craters >100 m						
Age of surface (Gyr)			1	2	3	4
Percent error of (one sigma certainty)	Number of craters >100 m to be counted	Number of craters* imposed on each km^2	3	6	9	12
10	100	Area to be used for crater counting (in respect to ages and confidence levels)	33	17	11	8
5	400		133	67	44	33
3.2	1000		333	167	111	83
1	10000		3333	1667	1111	833

For craters >500 m						
Age of surface (Gyr)			1	2	3	4
Percent error of (one sigma certainty)	Number of craters >500 m to be counted	Number of craters* imposed on each km^2	0.007	0.014	0.021	0.028
10	100	Area to be used for crater counting (in respect to ages and confidence levels	14286	7143	4762	3571
5	400		57143	28571	19048	14286
3.2	1000		142857	71429	47619	35714
1	10000		1428571	714286	476190	357143

For craters >1000 m						
Age of surface (Gyr)			1	2	3	4
Percent error of (one sigma certainty)	Number of craters >500 m to be counted	Number of craters* imposed on each km^2	0.001	0.002	0.003	0.004
10	100	Area to be used for crater counting (in respect to ages and confidence levels	100000	50000	33333	25000
5	400		400000	200000	133333	100000
3.2	1000		1000000	500000	333333	250000
1	10000		10000000	5000000	3333333	2500000

* Based on the lunar production function (Neukum et al 2001).
In calculations an assumption that the production function did not change was used, even though it is probably not valid for older ages when the production was higher. This would result in smaller minimal areas needed for satisfactory crater counts than presented above. Values presented above have to be treated as a maximal lowest area needed for crater count with specific error assumed, especially for older ages.

Crater morphology

Crater degradation state can be used to infer relative ages (Fig. 1.11). With time older craters appear more 'weathered' and their rims appear smoothed and less distinct due to the cumulative effects of superposed smaller impacts. Based on the amount of weathering and observed morphologic changes from the more 'fresh' appearance of newly-formed craters, it is possible to obtain a rough relative age of the crater. This approach can be used all over the Moon, on the near as well as on the far side, but this is not a precise dating method. The observed morphology of the crater can be influenced not only by the impact weathering process, but also by the effects of impacts in close proximity — for example, a crater covered by the ejecta blanket of another may appear older than it really is.

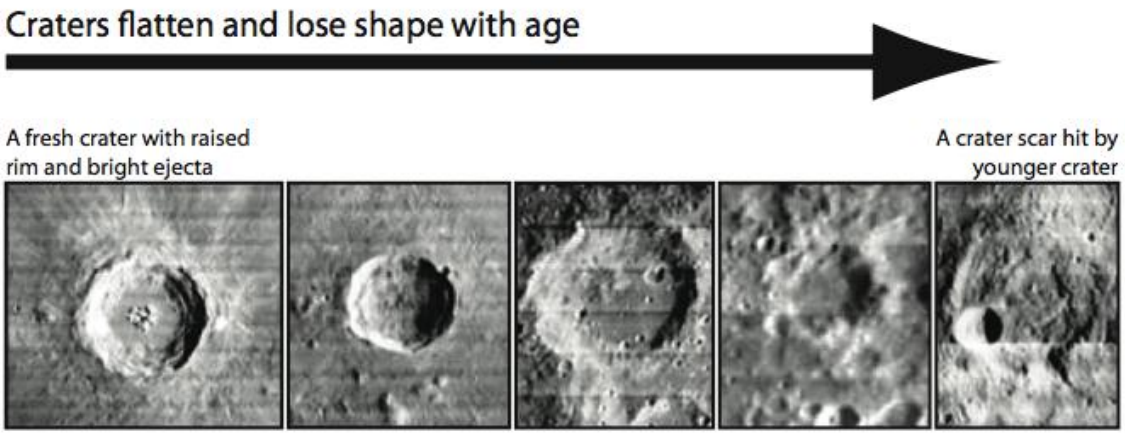

FIGURE 1.11 Evolution of crater morphology with time (Modified from classroom illustration by Paul Spudis).

Albedo and geochemical data

Crater rays fade with time (albeit at an as-yet unknown rate) and albedo differences and elemental data from remote sensing can be interpreted as indicative of age differences between mare units (Hiesinger *et al.*, 2001).

Exposure ages

Exposure age defines the time when a particular piece of rock has been exposed to cosmic rays for the last time. This method is limited to very young features, as was done during Apollo missions to date the young Copernican craters Cone, North Ray, and South Ray, and to date a landslide at the Apollo 17 site (Stöffler *et al.*, 2006).

Radiometric dating of returned samples

Lunar rock samples have been returned to Earth by six Apollo missions and 3 Luna missions. This permitted detailed laboratory studies, including radiogenic isotopic dating. These methods allow obtaining an absolute age of very small (micro grams) amounts of sample. Radiogenic isotopic dating techniques that are most widely used on lunar rocks include Rb-Sr, Sm-Nd, and Ar^{40}-Ar^{39} (Stöffler *et al.* 2006). They can be used to obtain crystallization ages as well as the ages of impact events by dating degassed melts produced during the impacts.

Establishing a precise absolute chronology by dating craters

Craters and impact basins cover most of the Moon's surface. Establishing the ages of specific craters and basins is important because their ages are the basis of the lunar chronologic system. The ages of a few important features have already been established (for example Imbrium basin), but ages of other significant features like Orientale have yet to be established. The age of the South Pole-Atkin basin, thought to be the oldest and largest basin on the Moon and, thus, a key anchor point in defining the lunar chronology, is still not known.

The distribution of some craters dated by various means (Wilhelms, 1987) is shown in Fig. 1.12. Most of the pre-Nectarian craters and basins are much larger than later ones. Small craters were formed during all periods, but they are in large part erased from the surface of the Moon by later impacts and so are preferentially represented in younger periods. The Imbrian is the last period when basins were created (Imbrium, Orientale, and Schrödinger).

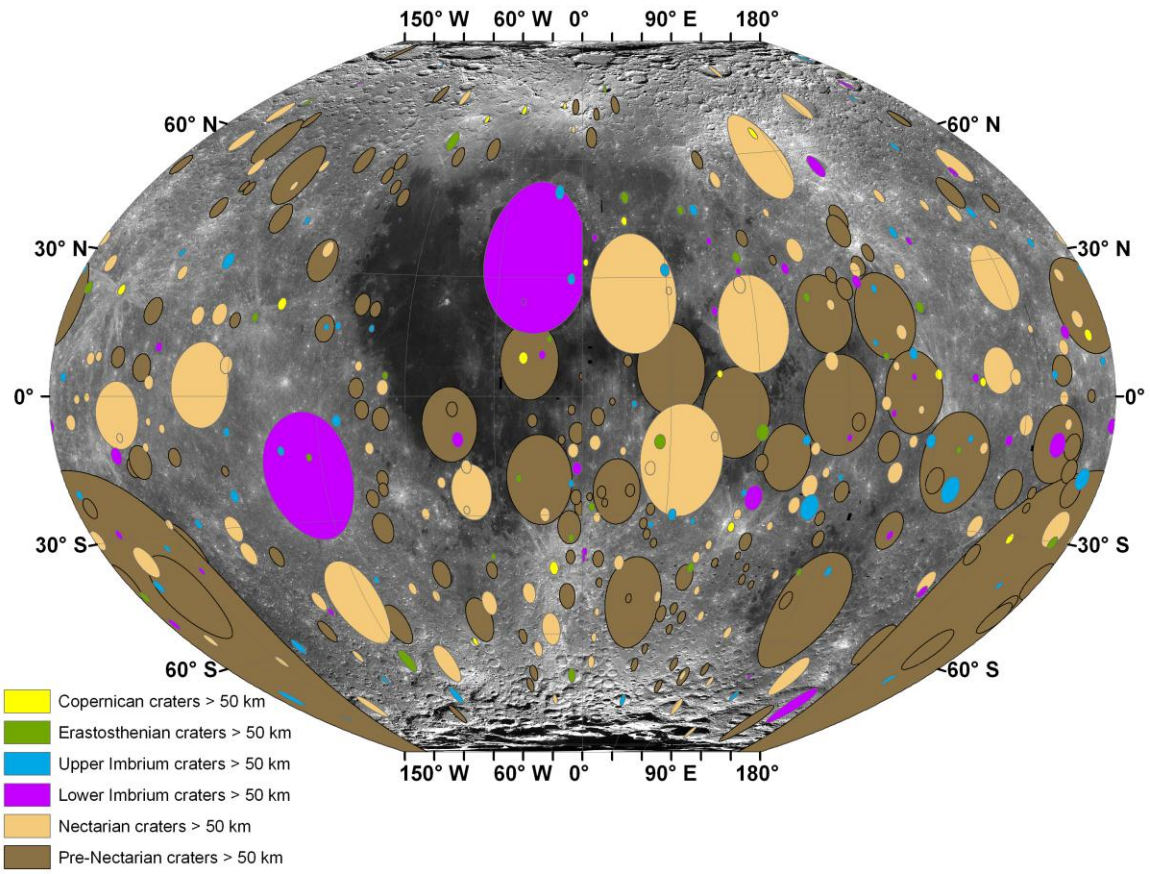

FIGURE 1.12 Map of lunar craters with assigned dates (only craters with dates presented in Wilhelms, 1987). Size of ellipses corresponds to the actual crater size.

Samples for radioisotopic dating of craters can be taken from various locations within and around craters. Each of the locations has advantages and disadvantages, so choosing a specific sampling approach should be tailored to the crater being sampled and considered together with site operational requirements and possibilities for obtaining other Science Concept Science Goals at the same site. Possible approaches for crater dating include:

1. Date melt present in the breccias in the crater floor

   All craters, including small, simple craters have breccias present in the crater floor.

   Advantages

   - Applies to all craters.
   - Extensive portion of the Moon is available for usage of this approach.
   - It gives a relatively high chance to correctly link a crater with the dated sample.
   - Broad flat floors of complex craters provide relatively safe landing sites.

   Disadvantages

   - The area in which sample can be collected is restricted to the crater interior (which in case of simple craters can be very small).
   - Not all melts from breccias are result of the impact that is being dated. The youngest melt fragment found should be the closest to the actual age of the impact, but if a very small sample (as for the robotic sample return mission) is returned, it is possible that chosen fragment does not contain melt of interest.

- A landing site located in the crater floor allows dating just one impact with high linkage potential. More impacts can be dated (multiple generations of impact melt) but their linkage potential is much lower.

2. Date breccias from ejecta blankets

   This approach can be applied to all craters, because all craters have ejecta blankets. The linkage potential of this method is highly variable and depends on age (dating of older craters is less certain), size (smaller craters have smaller ejecta blanket so they need to be sampled in proximity to the rim or a linkage between sample and feature is less certain), and history (craters overlaid with multiple later ejecta have less certain linkage between sample and crater).

   Advantages

   - Ejecta blankets cover much of the Moon, so a very large area is theoretically available for sampling.
   - Using high precision images (especially for younger or large craters), the provenance of ejecta blanket deposits can be determined with high certainty.

   Disadvantages

   - Ejecta blankets do not consist exclusively of material that had its radioisotopic clock reset during the formation of the crater, and much material included in the breccia is not influenced by the impact. During the emplacement of an ejecta blanket local material is entrained within it (*e.g.*, Oberbeck *et al.*, 1974; Li and Mustard, 2003). The farther away from the crater, the higher the amount of included local material. Glasses in the ejecta blanket can be either from the cratering event of interest or from an earlier one.
   - Ejecta blankets thin with the distance from the crater; in the proximity of the crater they are continuous. Obtaining a sample from the zone of continuous ejecta would allow dating the crater even if a small amount of sample is collected, so potentially robotic sample return mission should be efficient. Outside the zone of continuous ejecta blanket is a zone of discontinuous ejecta blanket where in some places local material is present on the surface. Finding the right spot on the discontinuous ejecta blanket for sampling requires detailed studies of orbital images.
   - The surface of the ejecta blanket may not be as flat as other types of surfaces (*e.g.* melt sheets); its topography can be very diverse and consist of large boulders. Not all areas within ejecta blanket are equally easy to land on.

3. Date impact melt sheets or ponds present in the floor, on the walls, or on the rim.

   This approach applies mostly to large craters that produce enough melt to develop extensive melt sheets or ponds. Relatively fresh craters (Copernican, younger Eratosthenian) have melt ponds well preserved on the surface. Older large craters and basins have extensive melt sheets in the floor, at least partially buried below later ejecta and/or mare basalts. Impact melt features are observed in craters as old as 3.5 Gy and ranging in size from 3 km to more than 200 km in diameter (Howard and Wilshire, 1975).

   Advantages

   - Melt ponds can be related to specific craters with very high probability.
   - Melt sheets and ponds are relatively flat, thus landing there and sampling is relatively easy.
   - Interiors of large craters offer other interesting features that can be used to accomplish many other scientific goals.

   Disadvantages

   - One landing site allows dating just one large crater (and possibly a few small ones).
   - Melt sheets of older craters are often covered by mare basalts or ejecta blankets. Thus it is necessary to excavate the melt layer from below by sampling ejecta of younger craters located inside the one to be dated that are large enough to have excavated deep enough to sample the melt sheet.

4. Date visible rays.

The approach of dating ejecta from visible rays applies only to young craters (Copernican).

Advantages

- Can be used to date craters that are very far away from the landing site (thousands of kilometers from the crater).

Disadvantages

- Low linking potential, least reliable. Quality of obtained date depends on a very precise orbital image analysis before picking a landing site, as well as very precise sample collection.

5. Obtain radiogenic exposure age of material ejected from craters.

   This method applies only to very young craters.

   Advantages

   - Very high linking potential.

   Disadvantages

   - Restricted to very young craters.

Using craters as reference surfaces

Melt sheets and ponds

Impact melt sheets and ponds can be used as reference surfaces for crater counting analyses. In most cases melt sheets or pond surfaces are rather flat, although ghost craters (secondary craters within the newly-formed primary crater that were formed by fragments ejected on very high-angle trajectories and then covered by melt flowing back from the walls of the crater) can sometimes be observed in them (Shoemaker *et al.*, 1994). Melt is developed in craters of all sizes, but only craters with diameter larger than ~50 km can have melt sheets (or ponds) that are large enough for statistically significant crater counting analyses (Table 1.4). Figure 1.13 shows a large melt pond in the north rim of King crater that has a size sufficient for crater counting work.

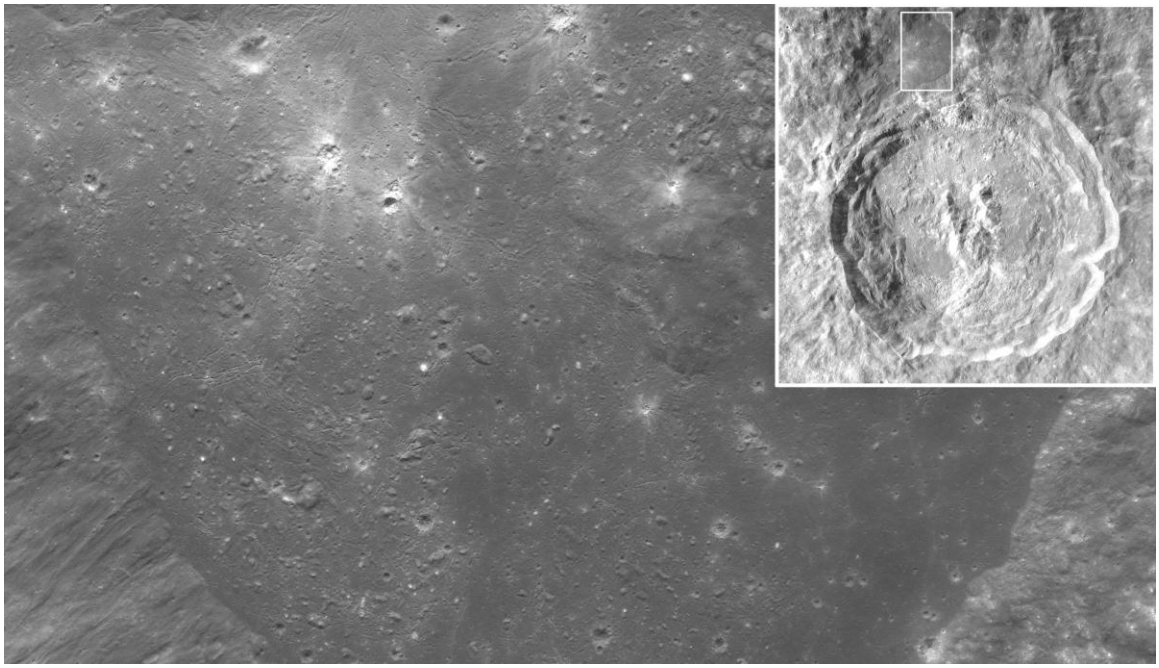

FIGURE 1.13 The cratered surface of the King crater melt pond. LROC NAC image M106088433L/R. Area indicated in inset image AS16-M-0891.

Melt sheets of very old craters can be covered by younger materials (ejecta blankets, mare basalts, etc.), that make them unsuitable for crater counting. But flat, extensive melt features have been recognized in craters as old as 3.5 Gyr (Howard and Wilshire, 1975). Tsiolkovskiy (Fig. 1.14) is a large (185 km diameter) Upper Imbrian crater with mare fill that has melt ponds preserved on its ejecta blanket.

FIGURE 1.14 Melt ponds on the rim of Tsiolkovskiy crater. The largest melt pond visible in the upper part of the image is ~10km in length. A15-P-9580.

Ejecta blankets

Ejecta blankets are also a type of reference surface, although the least preferred. They may exhibit significant topography and even initially are covered by secondary craters. Some of the secondary craters are easily recognizable, other are not so obvious. Ejecta blankets are used as reference surfaces because they cover large areas, and are uniformly distributed time and location. The absolute age of an ejecta blanket can be obtained by sampling material from the ejecta blanket itself, but also by dating the crater by any other method discussed above. For example, because melt sheets/ponds and the ejecta blanket are formed essentially simultaneously, by dating one it is possible to obtain an age of the other. If a crater has melt sheets or ponds of appropriate size, it is possible to compare results of crater counting for both surfaces and recalibrate other results.

Crater selection criteria

In the initial phases of future lunar surface exploration it will be impossible to date all or even most craters, so it is necessary to choose a representative group of craters best suited for dating to establish a precise absolute chronology. The results of dating those craters will be used to calibrate relative data methods across the entire Moon. Craters from the Lunar Impact Crater Database (Losiak *et al.*, 2009; Ohman, 2011) were selected and scored according to the following criteria:

- *Relation to the chronological time scale.* Craters used as markers in the lunar chronological time scale (*e.g.*, Nectaris, Imbrium, Orientale) or whose names define time periods (Eratosthenes, Copernicus) are given 20 points. They are the absolute priority.
- *Spatial distribution.* Craters of different sizes were chosen so they cover the surface of the Moon uniformly. Each chosen crater was given 10 points.

- *Size.* Larger craters are more useful for the chronologic and stratigraphic purposes because their ejecta cover much broader areas. Craters are assigned 1 point for each 20 km increment in diameter.
- *Included in "The geological History of the Moon".* Craters included in the representative craters tables prepared Wilhelms (1987) are assigned 1 point.
- *Typicality.* Craters listed as 'typical' in the representative craters tables prepared Wilhelms (1987) are assigned 3 points.
- *Age relation.* Craters with an age relation in the representative craters tables prepared Wilhelms (1987) are assigned 1 point.
- *Other.* Any important feature not included in the previous points. The number of points is subjective, but extensive explanation is included.
- *Dated.* Craters dated based on Apollo samples receive a number of points subjectively chosen based on validity of data.

Representative craters

For each time period groups of representative craters best suited for establishing a precise absolute chronology were selected based on the criteria described above. Maps of the selected representative craters are shown in Figs. 1.15–1.20. Basic characteristics of each named crater are tabulated in the Lunar Impact Crater Database (Losiak *et al.*, 2009; Ohman, 2011). Figure 1.12 above shows the combined map of the selected craters.

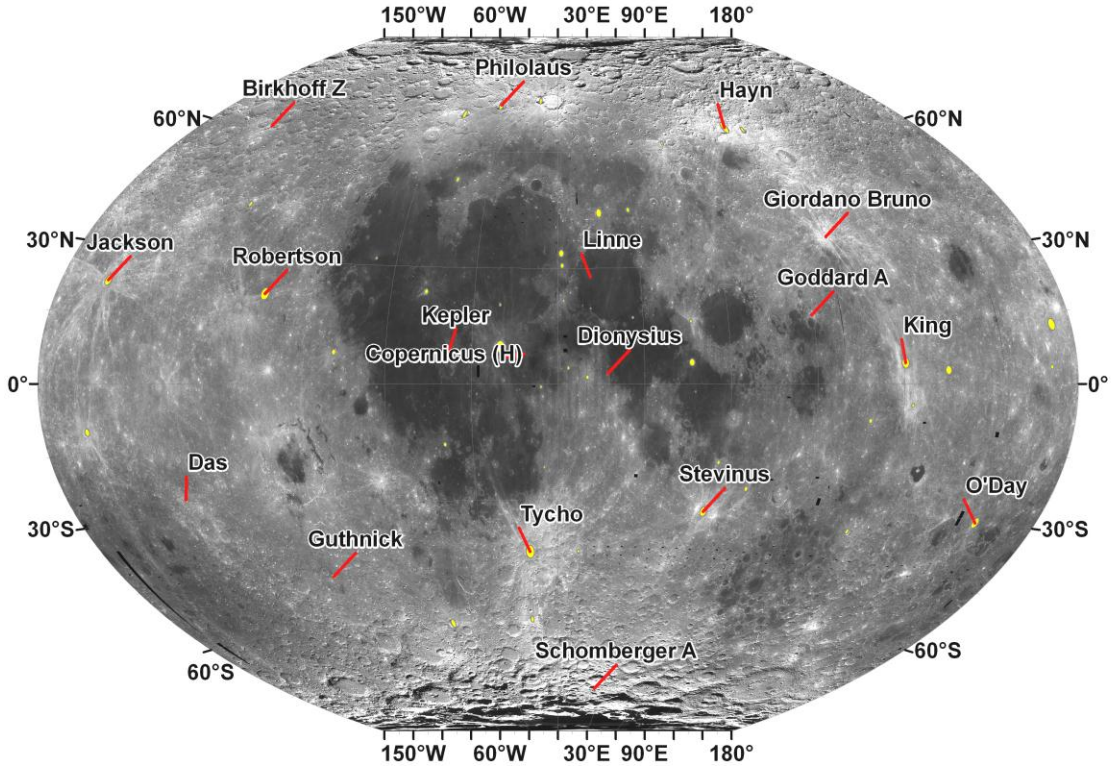

FIGURE 1.15 Map of representative Copernican craters.

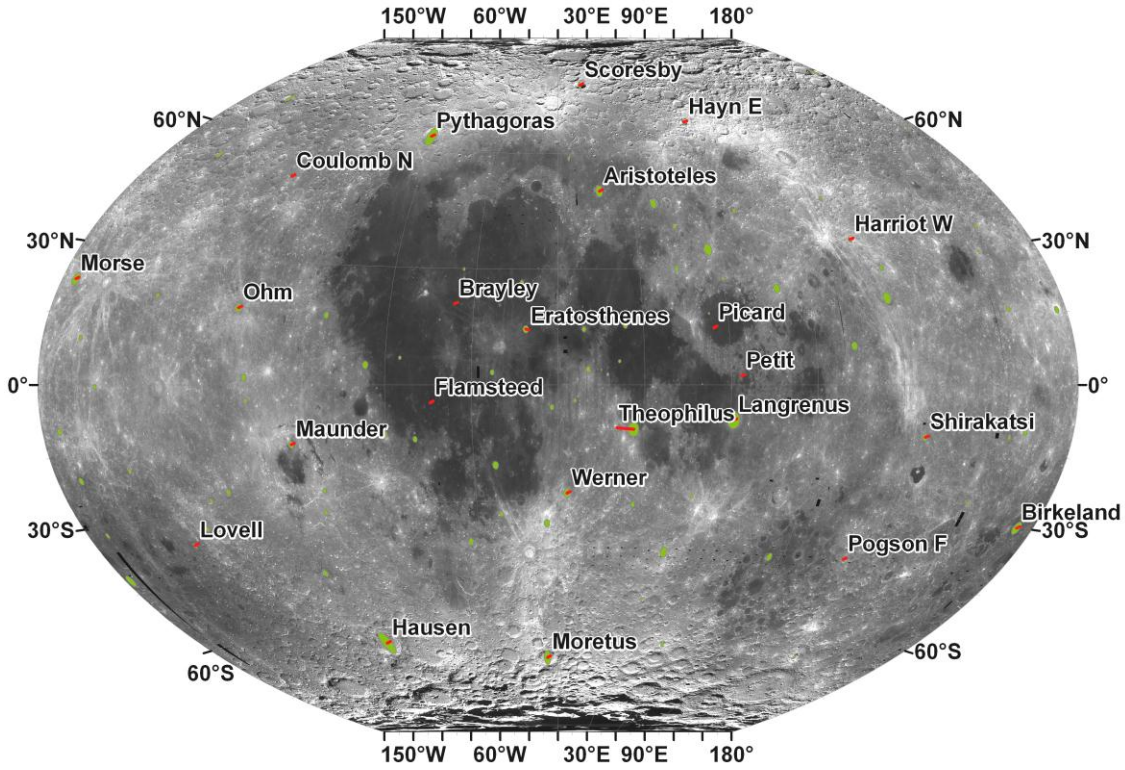

FIGURE 1.16 Map of representative Eratosthenian craters.

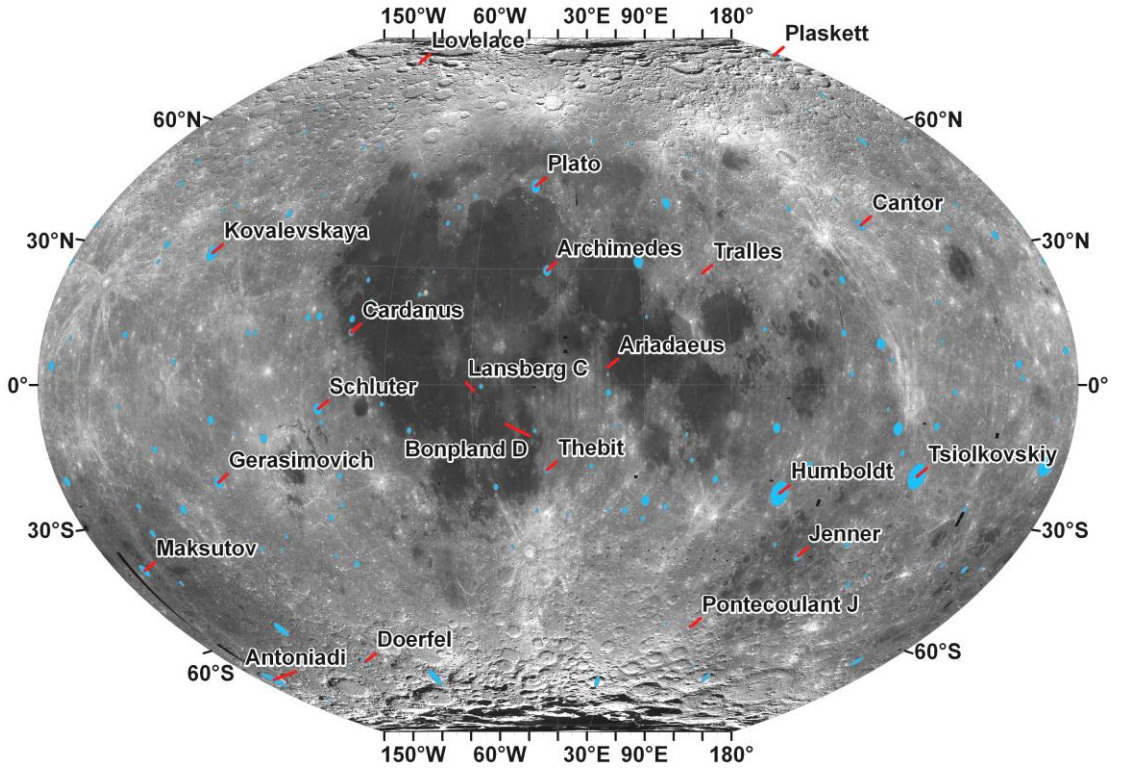

FIGURE 1.17 Map of representative Upper Imbrian craters.

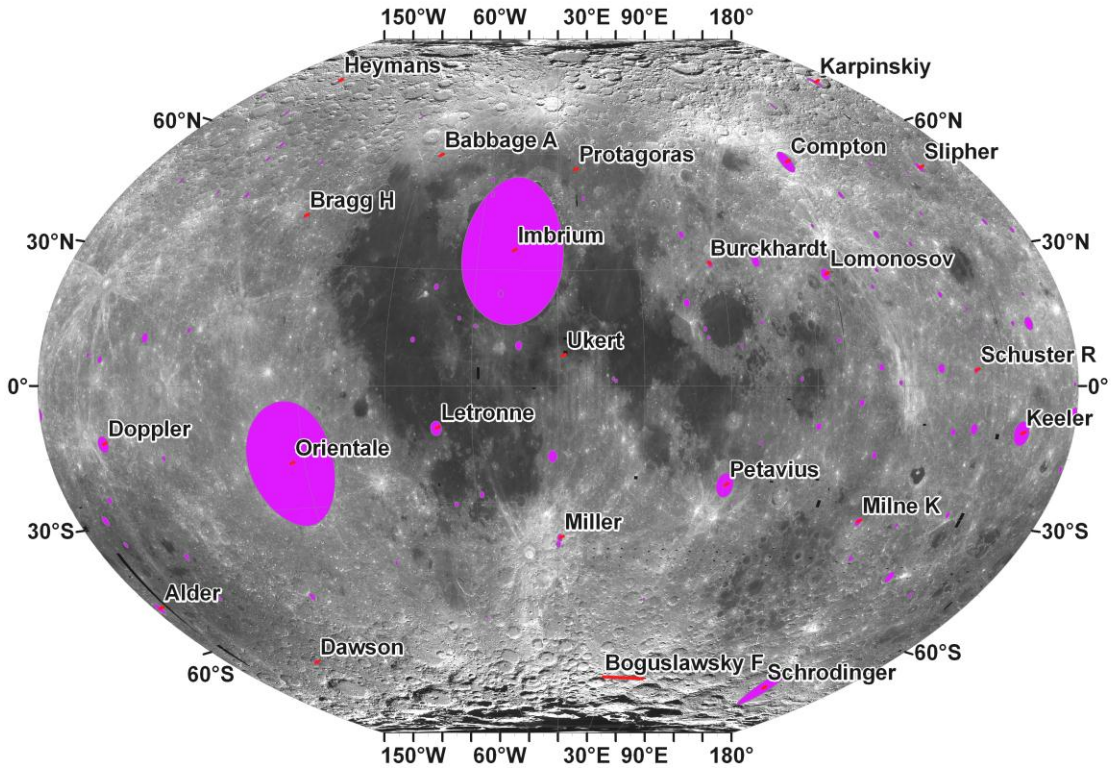

FIGURE 1.18 Map of representative Lower Imbrian craters.

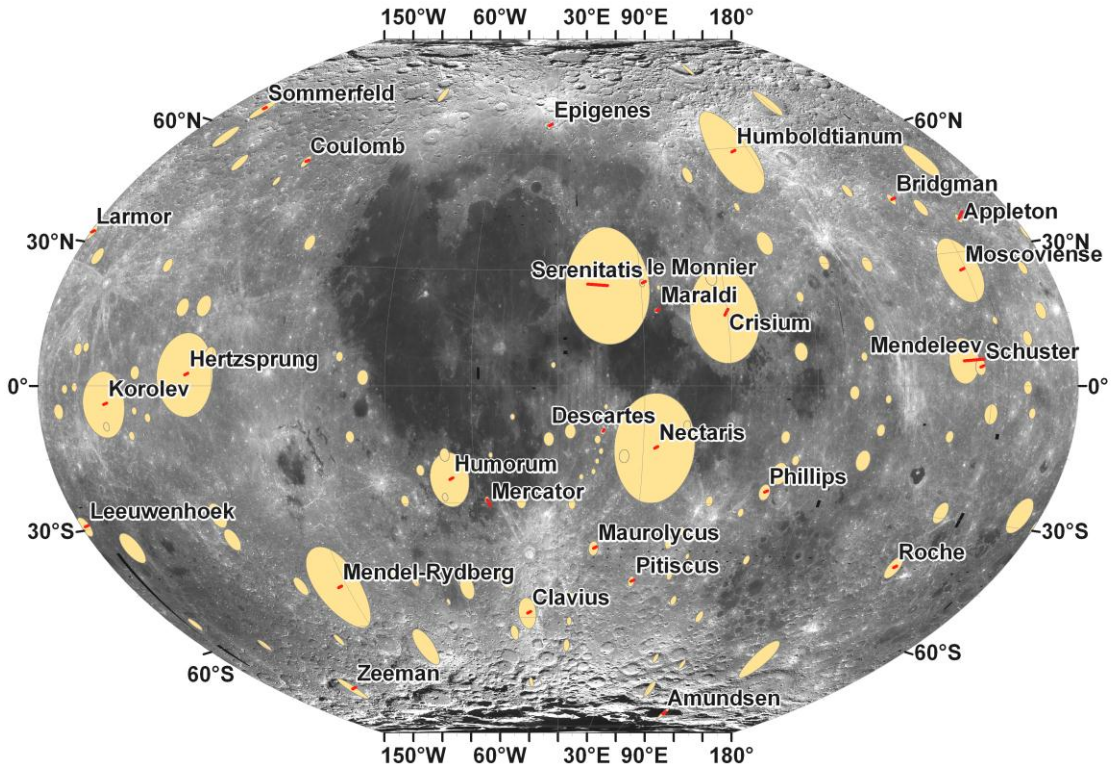

FIGURE 1.19 Map of representative Nectarian craters.

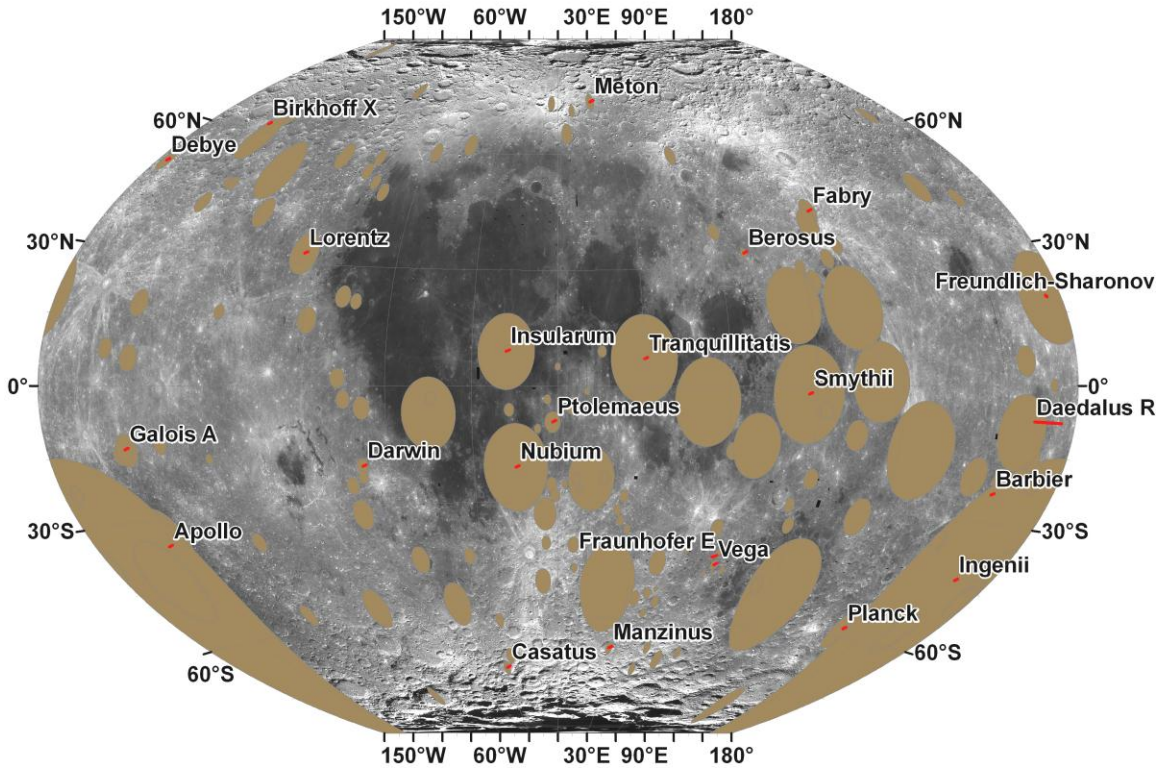

FIGURE 1.20 Map of representative pre-Nectarian craters.

Landing Site Example — Archimedes Crater

Archimedes (D = 82 km) is an Upper Imbrian crater located in eastern Mare Imbrium, ~260 km from the Apennine Mountains that mark the margin of Mare Imbrium (Fig. 1.21; *c.f.*, Fig. 1.17). Archimedes is superimposed on Imbrium basin and older mare basalt that is part of Appenine Bench Formation. Archimedes ejecta is covered by younger Imbrian mare; similar material fills the floor of the crater. Areas where Archimedes ejecta were not covered by mare deposits are visible on FeO and TiO_2 maps (Fig. 1.22). Younger craters of Eratosthenian and Copernican age occur on Archimedes ejecta deposits. Aristillus is a large (55 km diameter) Copernican crater with fresh morphology that is superimposed on the Archimedes ejecta blanket; it has no mare fill and is as deep as Archimedes (despite its smaller diameter).

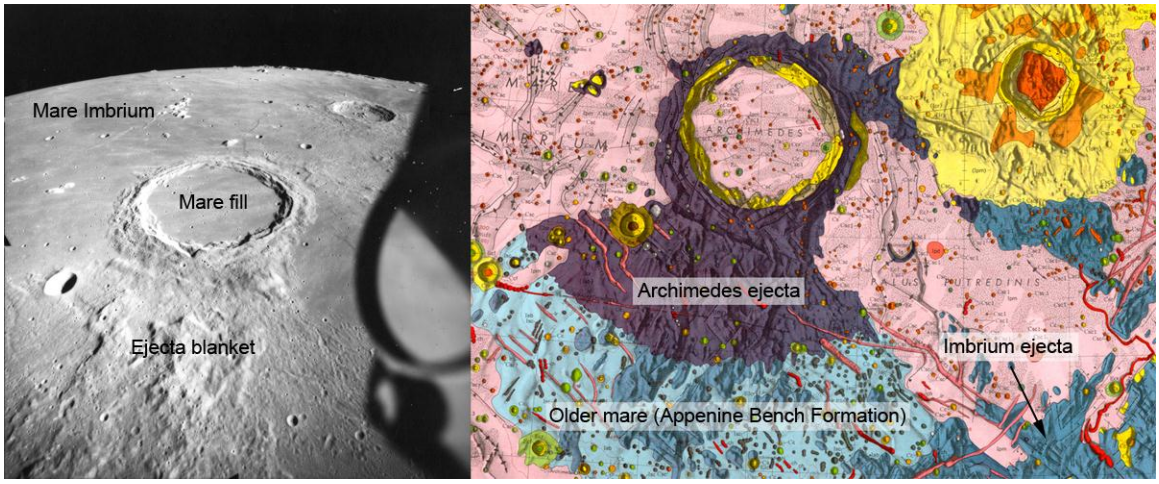

FIGURE 1.21 Left: The floor of Archimedes is filled with mare deposits. Mare basalts also cover part of its ejecta blanket. (AS15-M-1542). Right: Geologic map of the Archimedes area. USGS I-463.

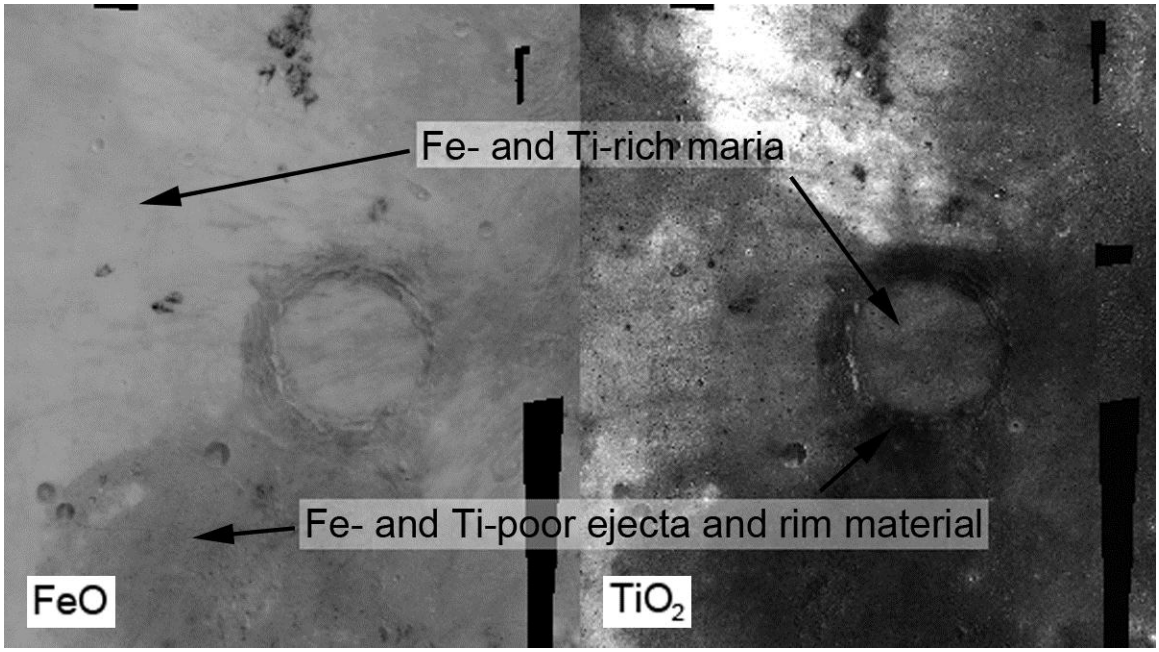

FIGURE 1.22 FeO and TiO2 abundance maps of the Archimedes area. Mare deposits are Fe- and Ti-rich, while the Archimedes ejecta blanket is Fe- and Ti-poor. Image based on The LPI Clementine Mapping Project.

Here we evaluate the five approaches for dating impact craters discussed above in the specific case of a large and relatively old crater like Archimedes:

1. Date melt present in the breccias in the crater floor.

   Archimedes-sized impacts produce large amounts of impact melt (1222 km^3 in the case of Archimedes; Cintala and Grieve [1998]) and breccias containing melt. In large craters breccias present in the crater floor can be covered by mare basalts. Excavation of the breccias from the crater floor in this case can be done only by craters large enough to penetrate to sufficient excavation depth (~2 km). Fragments of Archimedes breccias can be present on the surface in the elevated parts of the smaller craters, but they are not very abundant and may be covered by material slumped from the crater walls.

Finding: not recommended for dating complex and relatively old craters.

2. Date breccias from ejecta blankets

Archimedes has an extensive ejecta blanket that extends ~135 km from the crater center. Most of Achimedes' ejecta blanket was flooded by Imbrium mare basalt as well as partially covered by younger craters and ejecta blankets. Sampling must be proceeded by careful and detailed analysis of available data in order to exclude sites where ejecta of Archimedes are covered by younger features. Small-scale impacts do not reset the isotopic clocks of target material they excavate, so Archimedes melt may be found even in the ejecta blankets of Autolycus or Archimedes A. In those cases establishing which obtained date reveals the real date of Archimedes may be problematic, but with sufficient sample diversity it should be possible to distinguish between the different impact events with high probability. The safest approach would be to sample the ejecta blanket of a crater that is very young and dated in different way (*e.g.*, radiogenic exposure age) and subtract this date from the ones obtained by radioisotope dating. Another way to sample breccias from ejecta blankets of old craters is to sample regolith after verifying that the ejecta blanket of the crater is visible on the surface.

Finding: recommended for dating complex and relatively old craters.

3. Date impact melt sheets or ponds present in the floor, on the walls, or on the rim.

Craters larger than ~30 km in diameter often have melt flow structures visible on the surface (Howard and Wilshire 1975). Archimedes probably has an extensive melt sheet present in the floor of the crater; some melt could be preserved also on the walls as well as on the ejecta blanket proximate to the rim. Melt sheet material on the floor, as well as some present on the ejecta blanket, was flooded by the mare basalts, however. Melt from the rims and walls can be still present on the surface, although it covers relatively small areas, and additionally it can be relatively hard to identify (or impossible in older craters) because of space weathering.

In order to sample material from the Archimedes' extensive melt sheet it is necessary to excavate it from beneath mare basalts that may be as thick as 2 km, though it may be less thick near the crater rim. The excavation can be done by drilling or using crater ejecta. Using ejecta of craters from the crater interior is faster and easier. The two largest craters located inside Archimedes are Archimedes T and S. Both craters are located close to the rim of Archimedes where the mare basalt layers should be thinner, and have diameter of ~3 km, suggesting excavation depths of ~0.25 km. This excavation depth may be sufficient to penetrate below the mare basalts to Archimedes melt sheet materials. On the other hand, melt sheets are not distributed evenly in crater interiors, so it is possible that there is no melt sheet material below Archimedes T or Archimedes S. Unfortunately, other craters are so small that the chance that they have penetrated through the mare basalt is low. High-resolution elemental abundance maps could be used to verify if the excavation depth was sufficient to penetrate the mare cover.

Finding: recommended for dating complex and relatively old craters, if melt sheet material can be detected on the surface, or if younger craters penetrated through any mantling layers.

4. Date visible rays.

Old craters like Archimedes do not have a ray system that is easily recognizable and linkable with the source, because weathering has erased it from the surface.

Finding: not useful for dating craters older than Copernican (and some examples from Eratosthenian) age.

5. Obtain radiogenic exposure age of material ejected from craters.

Radiogenic exposure age can be fully reliable only for very young craters.

Finding: not useful for dating relatively old craters.

SCIENCE GOAL 1D: ASSESS THE RECENT IMPACT FLUX

Introduction

The scientific study of the Moon is intimately linked to geological research of the Earth itself. The Phanerozoic eon is the current eon of the terrestrial geologic timescale and the one through which complex life has existed. A corresponding period of time on the Moon is therefore thought to be a good approach for defining the term 'recent' in the context of this study. The Phanerozoic eon began at about 0.54 Ga; it does not have a precise equivalent (numerically) within the established geologic timescale of the Moon, but the Copernican is its counterpart as being the current lunar geological period. The term 'recent' is thus defined here as the Copernican period. As indicated in Fig. 1.23, the base of the Copernican is not properly defined or absolutely dated, but is thought to be at about 1 Ga. The crater Copernicus itself does not mark the period's base; it is merely a good early Copernican marker. Most Copernican craters exhibit bright ejecta rays, although this is not always the case. The period is ongoing and thus encompasses the present-day.

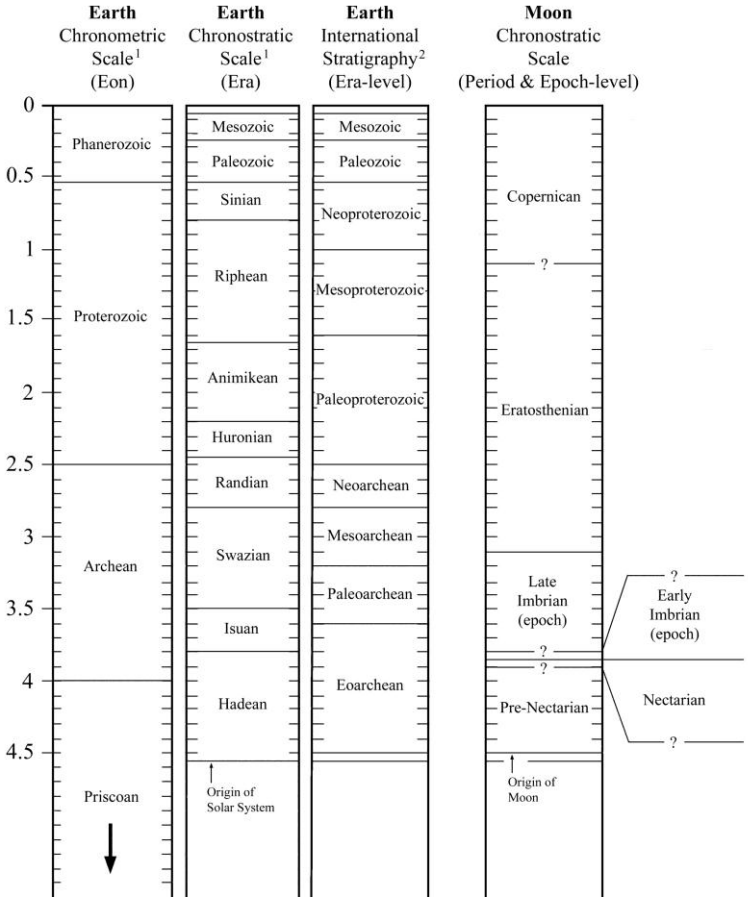

FIGURE 1.23. Comparison of the stratigraphic timescales of the Earth and Moon. (Unpublished diagram from Kring.)

To assess the recent impact flux, the distribution and effects of impacts on the lunar surface during the Copernican period must be studied. For these purposes the Copernican should be split into two distinct, yet overlapping parts:

1. the whole Copernican period
2. the very recent past and present day, *i.e.* the period of lunar exploration.

Whole Copernican period

The impact flux for the whole Copernican period can be estimated by determining the absolute ages of a set of representative Copernican craters. These can provide a basis and calibration for a new, accurate Copernican crater size-frequency distribution, which can be used to relatively date other Copernican craters. Crater counting is the standard method used for dating surfaces on the Moon and other solar system bodies. So that this can be achieved accurately, the flux of craters through time must be precisely known. By absolutely dating Copernican surfaces (of a significant area) on the Moon, crater densities for the Copernican can be established and thus the impact flux determined. These surfaces may be either impact material deposited from Copernican cratering events, or basalt flows emplaced during the period.

Period of lunar exploration

The impact flux during the period of lunar exploration can be directly assessed through comparison of old and new orbital imagery, in order to identify craters which have formed in the interim, and through deployment of seismometers as part of a global network, in order to detect the seismic waves created by meteoroid impacts (the site of the impact and the size of the meteoroid can thus be estimated).

Methodology

Absolute dating of representative craters

Choosing a representative set

Sixty one craters of diameter >2 km are identified as Copernican in age by Wilhelms *et al.* (1987). This list of craters was used as a basis for choosing a representative set of Copernican craters that could be dated in order to help assess the recent impact flux (Fig. 1.24 and Table 1.5).

Several criteria were used to identify craters which are representative in space, size, and relative age.

Space. The lunar surface was split into a grid with six latitudinal belts and eight longitudinal columns in order to identify a set of craters which were globally distributed.

Size. The craters were split into three groups according to their diameters (<15 km, 15–75 km, and >75 km) so that a range of sizes would be represented in the chosen subset.

Relative age. In Wilhelms *et al.* (1987) a certain number of the craters are recognized as being 'young' or 'very young' compared to the majority of the craters. This relative age classification was employed in choosing craters which were temporally widespread through the Copernican.

Target material. The target material into which the crater formed was also considered, a distinction being made between mare and nonmare material.

A total of ten craters (or pairs of craters) were chosen as the representative subset. When a pair of craters was chosen, this was because on the basis of these criteria, the two craters were identical. It should be emphasized that this subset is just an example of representative craters. Other criteria could be used and other representative craters thus be identified. An attempt was made to choose craters that were proportionally (± 10%) representative of the total dataset (*i.e.* if 10% of the sixty-two Copernican craters were less than 15 km in diameter, then 10% of the chosen subset should also be less than 15 km diameter).

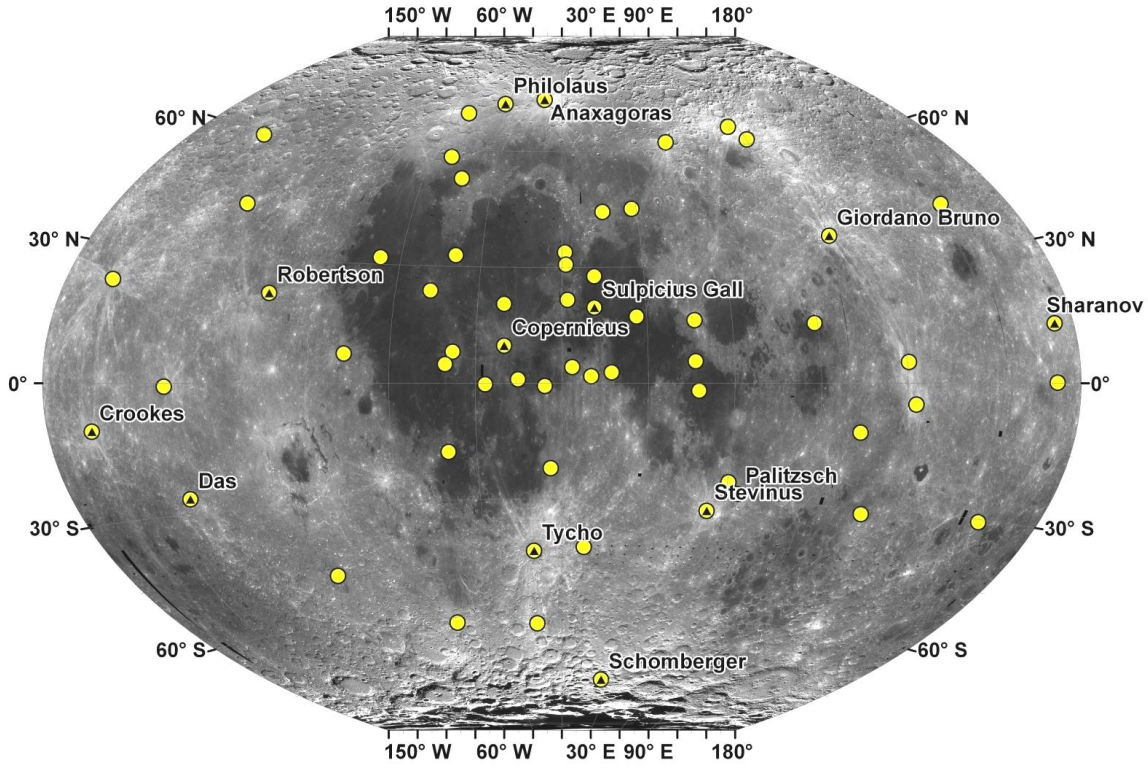

FIGURE 1.24 Map showing the 61 craters identified as Copernican (Wilhelms *et al.*, 1987; personal communication). Those craters which make up the chosen representative subset are marked by ▲ and are labeled (the crater Palitzsch is located beneath the Stevinus label).

TABLE 1.5 Sixty one craters identified as Copernican in age (Wilhelms *et al.*, 1987; personal communication) with their coordinates and diameters. Those highlighted are the craters that make up the chosen representative subset. Superscript numbers indicate pairs of craters that are identical in terms of the criteria used to the representative subset. § denotes 'young' craters and Ψ 'very young' craters as classified in Wilhelms *et al.* (1987).

Crater Name	Lat (°)	Long (°)	Diam (km)	Crater Name	Lat (°)	Long (°)	Diam (km)
[1]Anaxagoras	73.4	-10.1	50	Linné	27.7	11.8	2
Aristarchus[§]	23.7	-47.4	40	Maestlin	4.9	-40.6	7
Aristillus	33.9	1.2	55	Messier	-1.9	47.6	11
Autolycus	30.7	1.5	39	Milne (N)	-31.4	112.2	272
Bel'kovich	61.1	90.2	214	Mösting	-0.7	-5.9	24
Birkhoff (Z)	58.7	-146.1	345	Necho	-5	123.1	30
Bürg	45	28.2	39	O'Day	-30.6	157.5	71
Carpenter	69.4	-50.9	59	Olbers[§]	7.4	-75.9	74
Conon	21.6	2	21	[4]Palitzsch	-28	64.5	41
Copernicus	9.7	-20.1	93	Pasteur (D)	-11.9	104.6	224
Coriolis (Y)	0.1	171.8	78	Perrine	42.5	-127.8	86
[2]Crookes	-10.3	-164.5	49	Petavius (B)[§]	-25.1	60.4	188
[2]Das	-26.6	-136.8	38	[1]Philolaus	72.1	-32.4	70
Dawes	17.2	26.4	18	Proclus[§]	16.1	46.8	28
Dionysius[§]	2.8	17.3	18	Pytheas	20.5	-20.6	20
Eudoxus	44.3	16.3	67	Robertson	21.8	-105.2	88
Faraday	-42.4	8.7	69	Rutherfurd	-62.2	-11.9	10
Gambart	1	-15.2	25	Schomberger	-76.7	24.9	85
Gassendi	-17.6	-40.1	101	Sharonov	12.4	173.3	74
Giordano Bruno[Ψ]	35.9	102.8	22	South	58	-50.8	104
Goddard[Ψ]	14.8	89	89	[4]Stevinus	-32.5	54.2	74
Godin	1.8	10.2	34	Sulpicius Gallus	19.6	11.6	12
Gruithuisen	32.9	-39.7	15	Taruntius	5.6	46.5	56
Guthnick	-47.7	-93.9	36	Thales	61.8	50.3	31
Harpalus	52.6	-43.4	39	Thebit (A)	-22	-4	56
Hayn	64.7	85.2	87	Triesnecker	4.2	3.6	26
Jackson	22.4	-163.1	71	Tycho[§]	-43.4	-11.1	85
Kepler[§]	8.1	-38	31	Vavilov	-0.8	-137.9	98
King	5	120.5	76	Von Neumann	40.4	153.2	78
Lansberg (B)	-0.3	-26.6	38	Zucchius	-61.4	-50.3	64
Lichtenberg[§]	31.8	-67.7	20				

Landing Site Example —Tycho Crater

Tycho has a diameter of 85 km and a depth of about 4.5 km (Figs. 1.25 and 1.26). It is located at 11.1°W and 43.4°S. It is the youngest large crater on the nearside of the Moon with a conspicuous ray system. Tycho is thought to have been absolutely dated, from a sample collected during Apollo 17 from the slope of the South Massif. It is believed that a landslide was triggered by the ejecta of Tycho (2200 km away). The landslide material has an exposure age of about 0.1 Ga (Wolfe *et al.*, 1975; Arvidson *et al.*, 1976; Drozd *et al.* 1977; Lucchitta 1977) and this age has therefore been proposed for Tycho. Because the age is indirectly determined, confirmation with samples at Tycho is warranted.

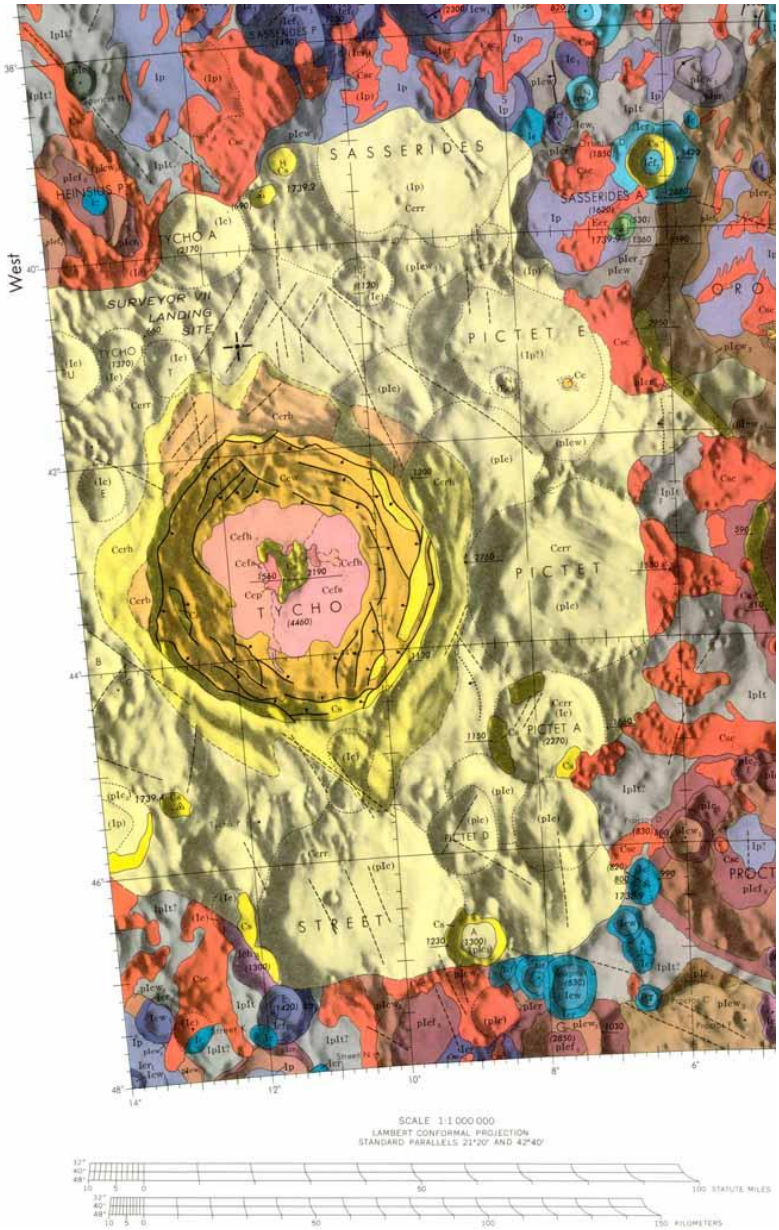

FIGURE 1.25 A portion of the geologic map of the Tycho quadrangle of the Moon, showing Tycho itself. Geologic units of importance are described in Table 1.6 (Pohn, 1972).

Figure 1.25 illustrates the geology of Tycho, as constructed from Lunar Orbiter images, and shows three units of ejecta deposits (*Ccrb*, *Ccrh*, *Ccrr*). An inner hummocky zone consists of units *Ccrb* (blocky rim material) and *Ccrh* (hummocky rim material), with a maximum extent is about 20 km from the crater rim. An outer, radial zone is made up of unit *Ccrr* (radial rim material) and accounts for much of the Tycho ejecta; it extends for about one crater diameter.

TABLE 1.6 Description and interpretation of important geologic units in Fig. 1.25 (Pohn, 1972).

Unit name	Characteristics	Interpretation
Cs	Material on steep slopes, primarily crater walls,	Bedrock and blocky talus exposed by

	distinctly brighter than Tycho ray material.	impact, faulting, and mass wasting.
Ccfs	Floor material, smooth. Few hummocks. Traversed by numerous fissures tens of meters wide barely visible on Orbiter IV resolution (about 100 m) but apparent on Orbiter V photographs (resolution ¼ m). Density of craters <1 km diameter lower than on crater rim.	Post crater lava or other volcanic filling subsequently cut by tension cracks as result of cooling.
Ccfh	Floor material, hummocky. Broadly rounded hummocks ¼ to 3 km diameter. Numerous fissures tens of meters wide. Density of craters < 1 km lower than on rim.	Post-crater viscous volcanic filling. Hummocks may be volcanic domes. Fissures possibly caused by calescence of individual volcanic elements. Some craters in floor may be effusion vents.
Ccrb	Rim material, blocky. Coarse and rather angular hummocks about ½ km diameter adjacent to rim crest.	Impact ejecta consisting mainly of large jumbled blocks swept clean of base-surge deposits.
Ccrh	Rim material, hummocky. Large subdued hummocks, about 5 km diameter, and subdued ridges subconcentric to rim crest. Heavily lineated in part. Distal to unit Ccrb where that unit present.	Impact ejecta covered by moderately thin blanket of fine material deposited from base surge.
Ccrr	Rim material, radial. Continuous surface having ropy or braided texture radial to Tycho. Subdued satellitic craters abundant (but not mapped) near outer contact; grades outward into facies dominated by satellitic craters (unit Csc)	Impact ejecta deposited by base surge.
Ccw	Wall material. Finely hummocky material on terraced wall. Small irregular and locally sinuous ridges and rimmed valleys trend down steep slopes.	Slumped rim materials and talus. Radial channels and ridges possibly formed by downslope movement of particulate material while crater interior still hot from impact shock melting.
Ccp	Peak material. Sharply angular complex of ridges and peaks near centre of carter.	Part of lens of intensely brecciated material uplifted immediately after excavation of crater; possibly later volcanic material in part.
Csc	Satellitic crater material. Material of small generally sharp-rimmed craters in clusters and string subradial to crater Tycho; craters are elongate or round single craters or coalescing craters. Many strings exhibit a herringbone or braided pattern splaying outward from Tycho.	Material of secondary impact craters produced by ejecta from Tycho. Some patches stop abruptly at crater rim crest facing Tycho but recur on floors and opposite walls, indicating ballistic shadowing – ejecta impacted surface at angle less than slope of walls.

Howard and Wilshire (1975) documented photographic evidence of once-fluid materials that ponded and flowed downhill, interpreted as localities of impact melt material. They describe four distinctive morphologies of these features, all of which have been identified within the ejecta deposits of Tycho:

1. *Superposition as a veneer over irregular surfaces*: A veneer of the impact material is draped over the inner part of Tycho's crater rim. A cracked veneer (feature labeled 1 in Fig. 1.27) on the main crater rim contrasts with blocky areas where no cracks occur (feature labeled 2 in Figure 1.27).
2. *Flow lobes and channels:* Leveed flow channels and lobes indicate that melt material flowed downhill both outside craters on the rims and inside on the walls (see Fig. 1.28).

3. *Complexly fractured pools on crater floors*: Thicker accumulations of fluid material, characterized by complex floor patterns of blocky cracks and wrinkelike corrugations, and by a somewhat knobbly yet generally level surface, flood the crater floor. The cracks in the material commonly continue over hummocks in the floor, indicating that the fluid material mantled these hummocks. In Tycho some hummocks are surrounded part of the way up by concentric shells implying that the tops of the hummocks are not coated (Kosofsky and El-Baz, 1970) (see Figs. 1.29 and 1.30). Fissured lavalike material forms isolated terraces along the edges of Tycho's crater floor (Strom and Fielder, 1970) (see Figs. 1.29 and 1.31).
4. *Smaller ponds on crater walls and rims*: Fluid material that ponded to a level surface occupies numerous small depressions on crater walls and rims (feature labeled 3 in Fig. 1.27). Most ponds are several hundred meters to several kilometers across, but some are much larger. Ponds on the rims of larger craters such as Tycho represent the greatest concentrations of, and the most fluid impact melt material. For Tycho, Shoemaker *et al.* (1968) estimated 120 km^3 of such materials on the rim and suggested that a comparable amount may be present on the floor. The largest rim pools are concentrated on the east side of Tycho where the ray pattern is most extensive.

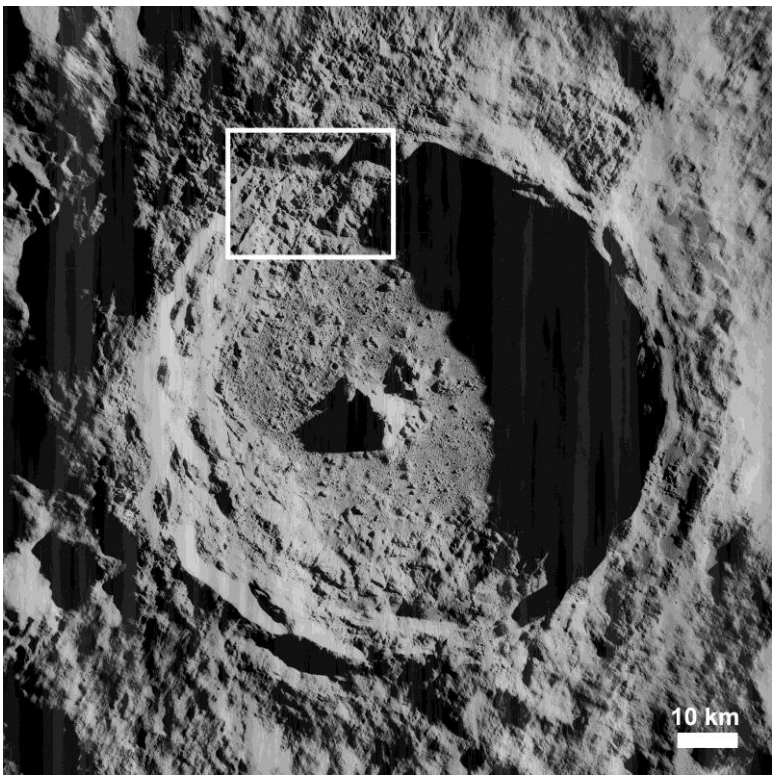

FIGURE 1.26 Lunar Orbiter image LO-V-125-M showing the crater Tycho. The box indicates the approximate position of the area shown in Fig. 1.28.

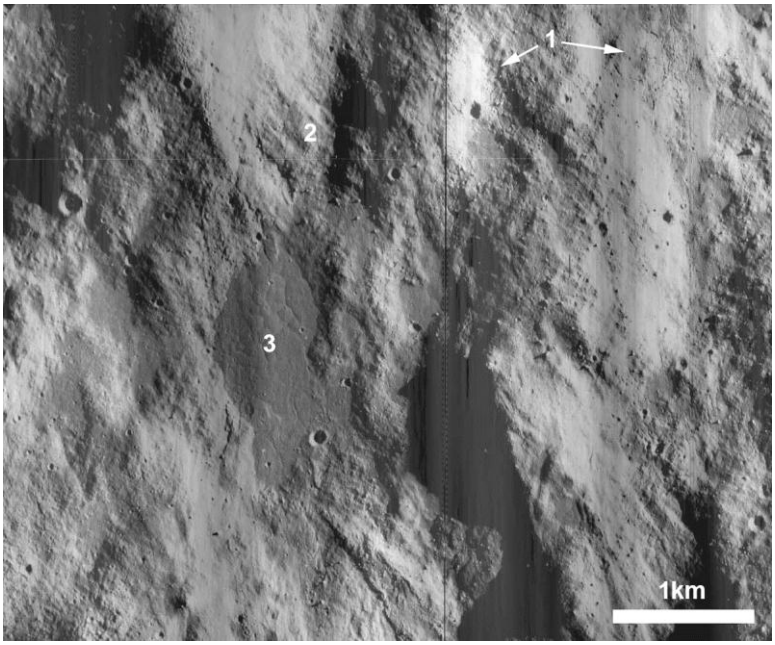

FIGURE 1.27 An enlarged portion of Lunar Orbiter image LO-V-127-H2 showing veneer, pools, and blocky areas on the north rim of Tycho. A cracked veneer (1) drapes the landscape and elsewhere blocky residues (2) are present where fluid material apparently drained toward pools. A large pool (3) has polygonal cracks.

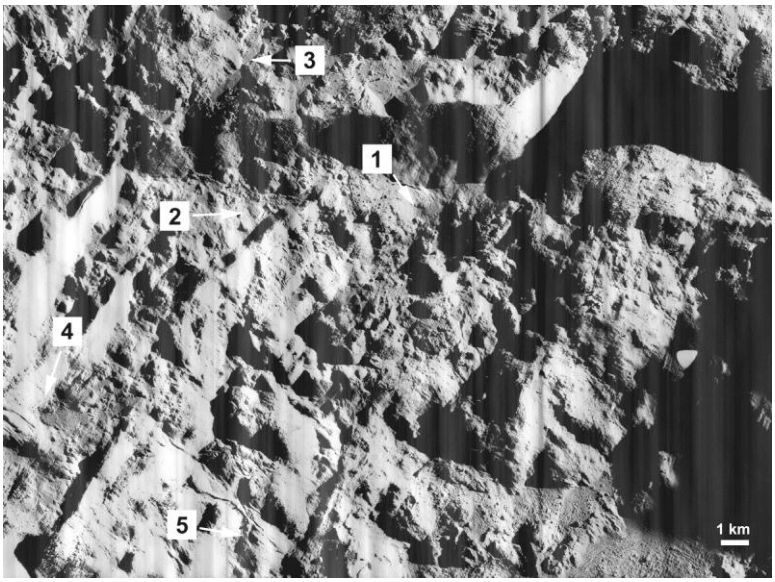

FIGURE 1.28 Lunar Orbiter image LO-V-126-H2 showing two flow features (labeled 1 and 2) which exhibit successive flow fronts, transverse ridges and fractures (parallel to the direction of flow and probably later features). A breach in the scarp to the north-west (labeled 3) may be a channel through which molten rim material flowed to form this front. Close examination of the rim reveals considerable pooling of material and patterns indicative of flowlike movement. The lower portion of the photograph (labeled 4) provides excellent examples of pools on a terrace interconnected by flow features. Flow levees (labeled 5) are well displayed and smooth-appearing flows with well-defined termini typically fill local depressions.

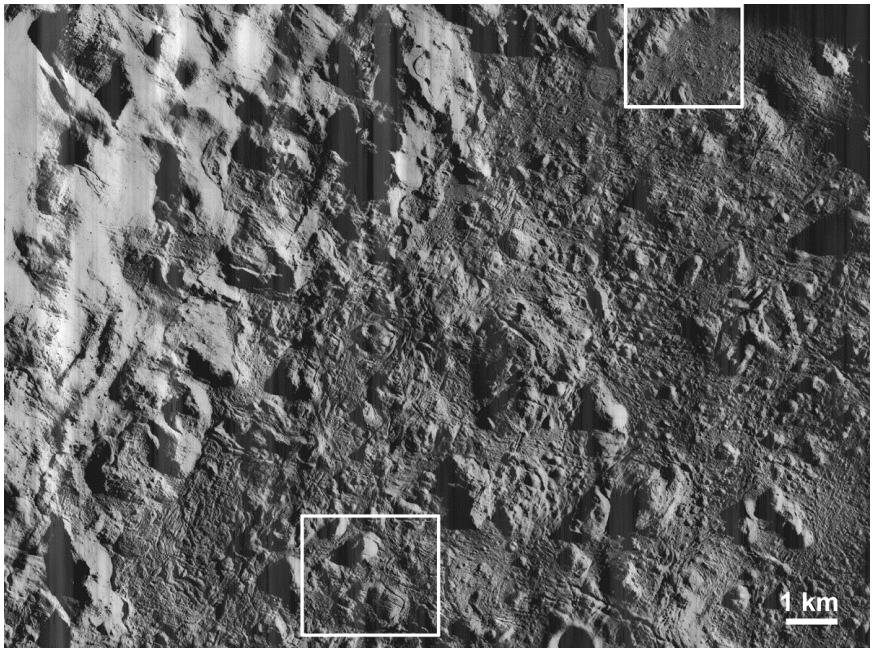

FIGURE 1.29 Lunar Orbiter image LO-V-125-H2 showing the north-western part of the floor and lower wall of Tycho. Boxes indicate the positions of Fig. 1.30 (bottom) and Fig. 1.31 (top).

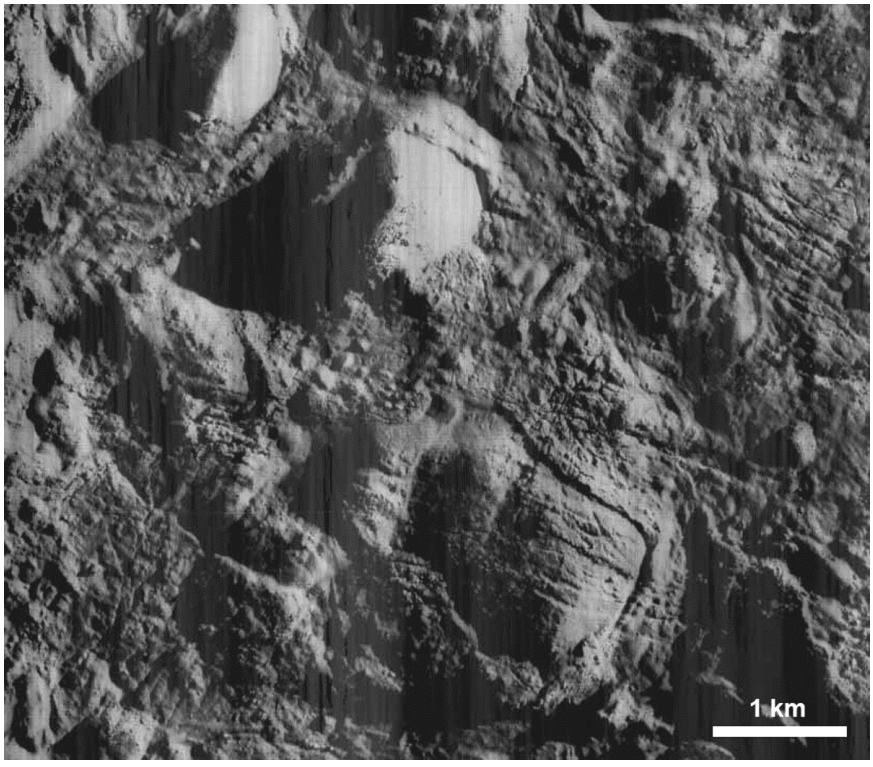

FIGURE 1.30 An enlarged portion of the bottom section of Fig. 1.29, showing a view of some of the roughest parts of the floor of Tycho. The symmetrical rings or shells surrounding the large mounds are thought to be due to the flow of shock-melted rock off the surface of the mounds. Fissures and blocks are abundant in all parts of the floor.

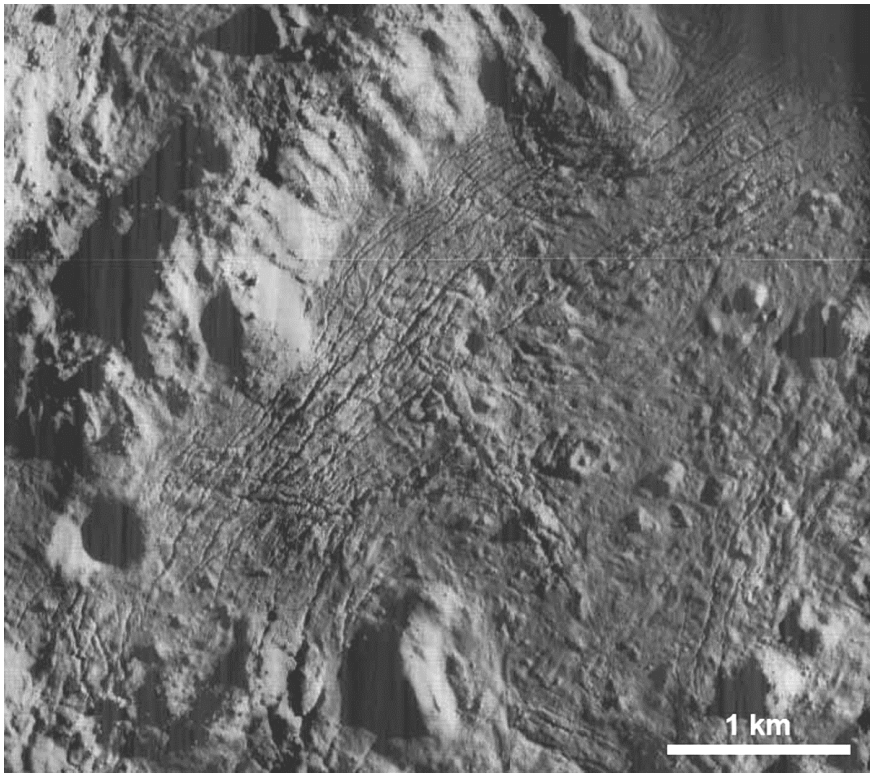

FIGURE 1.31 An enlargement of the north-eastern corner of Fig. 1.29, showing typical details of the floor and floor-wall contact of Tycho, including mounds, fissures, and blocks. Long fissures commonly parallel the floor-wall contact, while shorter, more irregular ones have variable directions. A flow lobe in the upper right corner has moved down the wall and 'bulldozed' its way into the floor material.

Hirata *et al.* (2000) use Clementine multi-spectral data (primarily the 750/415 nm ratio to recognize glassy material) together with Lunar Orbiter images to study the ejecta deposits of Tycho. They organize the ejecta into three categories:

1. Glassy ejecta containing a large amount of impact melt, with hummocky or radial surface texture.
2. Non-glassy ejecta seen only in the north rim, corresponding to the blocky rim material.
3. Massive melt deposits made of crystalline melt.

Suitable landing sites can thus be identified by combining the study of high-resolution imagery and multi-band spectral data to find localities of abundant melt material for collection and sampling.

Surveyor VII landed on the north flank of Tycho (the landing site is shown in Fig. 1.25) in 1968 and returned over 20,000 images from its television camera. Figure 1.32 is a mosaic of some of those images and gives an impression of the landscape surrounding the landing site.

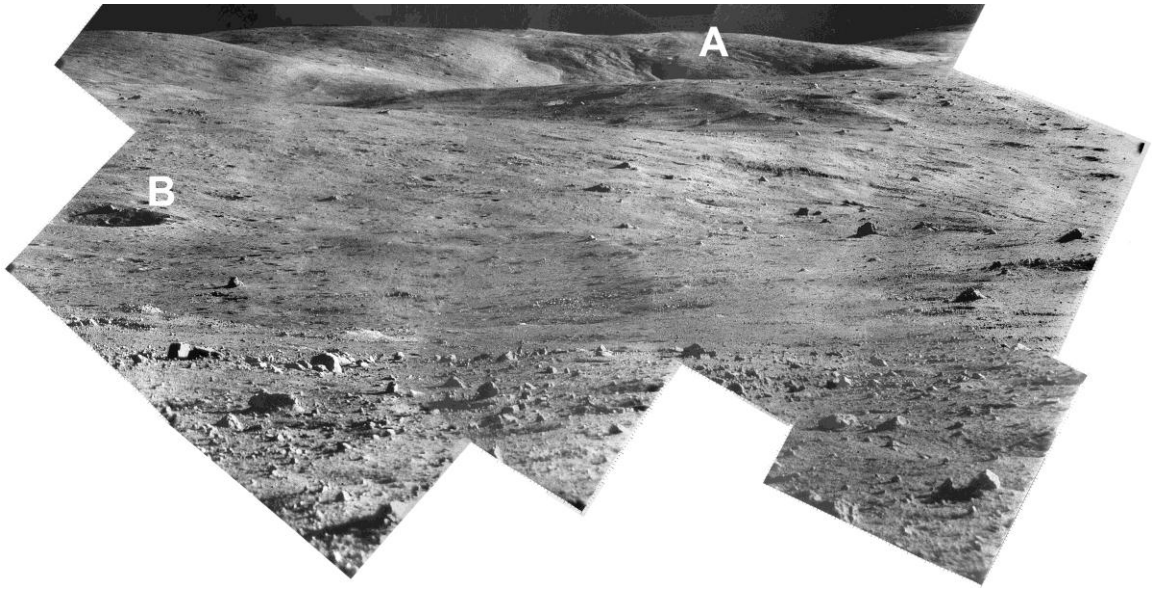

FIGURE 1.32 A mosaic of Surveyor VII narrow-angle pictures looking approximately north from the landing site (40.95°S, 11.41°W). The ridge labeled A is 21 km from the spacecraft and the crater labeled B is about 590 m from the space craft. Image courtesy of P. Stooke (University of Western Ontario).

Absolute dating of large scale Copernican surfaces

Absolute dating of Copernican deposits provides surfaces upon which to base calibrated crater counting. Other areas of the Moon can thus be relatively dated and the Copernican impact flux investigated. The surfaces must be homogenous on a scale with a large enough surface area to conduct statistically significant crater counts. Their horizons should also be stratigraphically important. These surfaces may be:

1. Ejecta blankets and floors of the representative Copernican craters identified above (or any other representative set), or
2. Basalt flows that were erupted and emplaced during the Copernican period.

Although widespread lunar volcanism is not thought to have occurred during the Copernican period, some authors have proposed that a number of basalt flows within Oceanus Procellarum are indeed Copernican in age. Schultz and Spudis (1983) claimed that lunar mare volcanism occurred continuously from before 4.1 Ga to as recently as 1.0 Ga (Copernican period). Some mare units are thought to overlap the bright ejecta rays of the Copernican crater Lichtenberg (67.7°W, 31.8°N), and thus are themselves Copernican (Moore, 1967). This stratigraphic relationship was confirmed in Lunar Orbiter images (Schultz, 1976) as shown in Fig. 1.33.

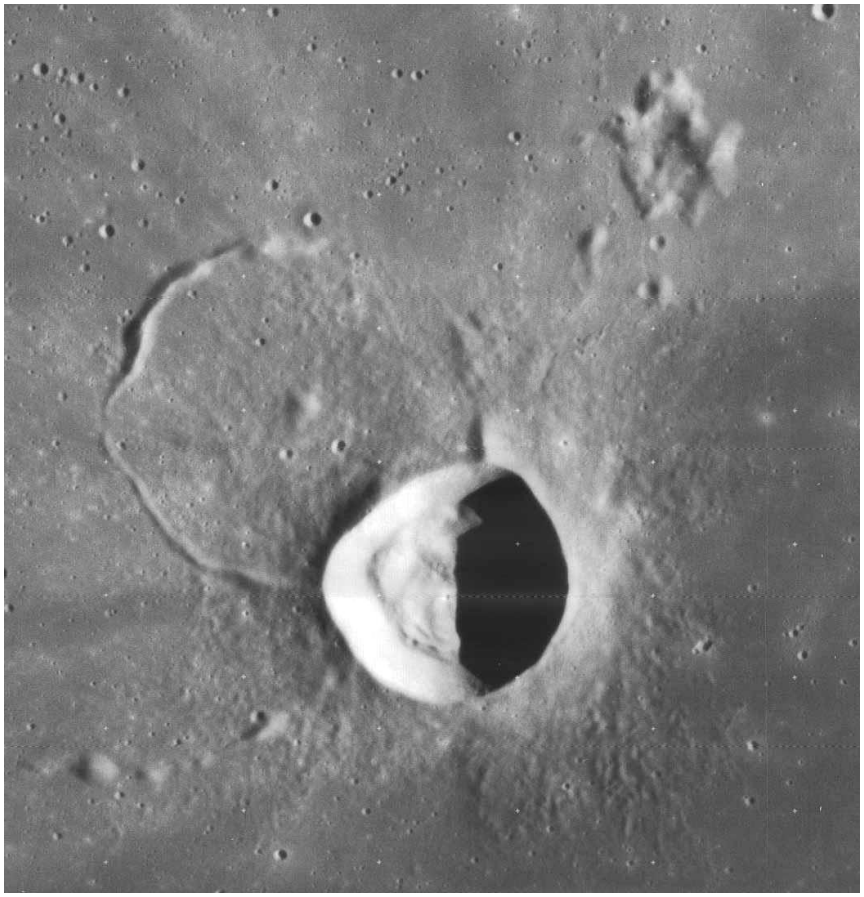

FIGURE 1.33. Lunar Orbiter image LO-IV-170-H1 of Lichtenberg crater, showing embayment of basalt flows on the eject blanket (bottom right).

Hiesinger *et al.* (2003) mapped individual basalt flows (Fig. 1.34) within Oceanus Procellarum (as well as other maria) using a Clementine multispectral high-resolution color ratio composite. They counted craters in areas within a number of these flows, employing the chronostratigraphic system of Neukum and Ivanov (1994). They thus identified five of the flows as Copernican in age. However, if other chronostratigraphies were utilized (*e.g.* Wilhelms *et al.*, 1987; Stöffler and Ryder, 2001), these same flows would instead be classified as Eratosthenian or Imbrian in age.

In order to absolutely date surfaces for crater counting purposes, any basalt material from these flows can be collected and returned to Earth for Ar-Ar dating. The oldest of these flows (labeled '1' on Fig. 1.34) should at least be visited and dated. If it is confirmed as Copernican in age, it follows that all the younger flows would also be. If, however, it is not Copernican the other flows (especially the youngest) would need to be dated in order to confirm the period over which they were erupted. This oldest flow is outlined in Figs. 1.35 and 1.36 on both existing geologic maps and Lunar Orbiter IV images. As can be seen in Fig. 1.35, the coverage of this entire area with published, detailed geologic maps is not complete. These are required for those areas for which they do not currently exist. The outlines and ages of flows mapped by Hiesinger *et al.* (2003) and on the geologic maps do not match because different resolution imagery and data types were used in their identification (Clementine UVVIS and Lunar Orbiter / telescopic observations).

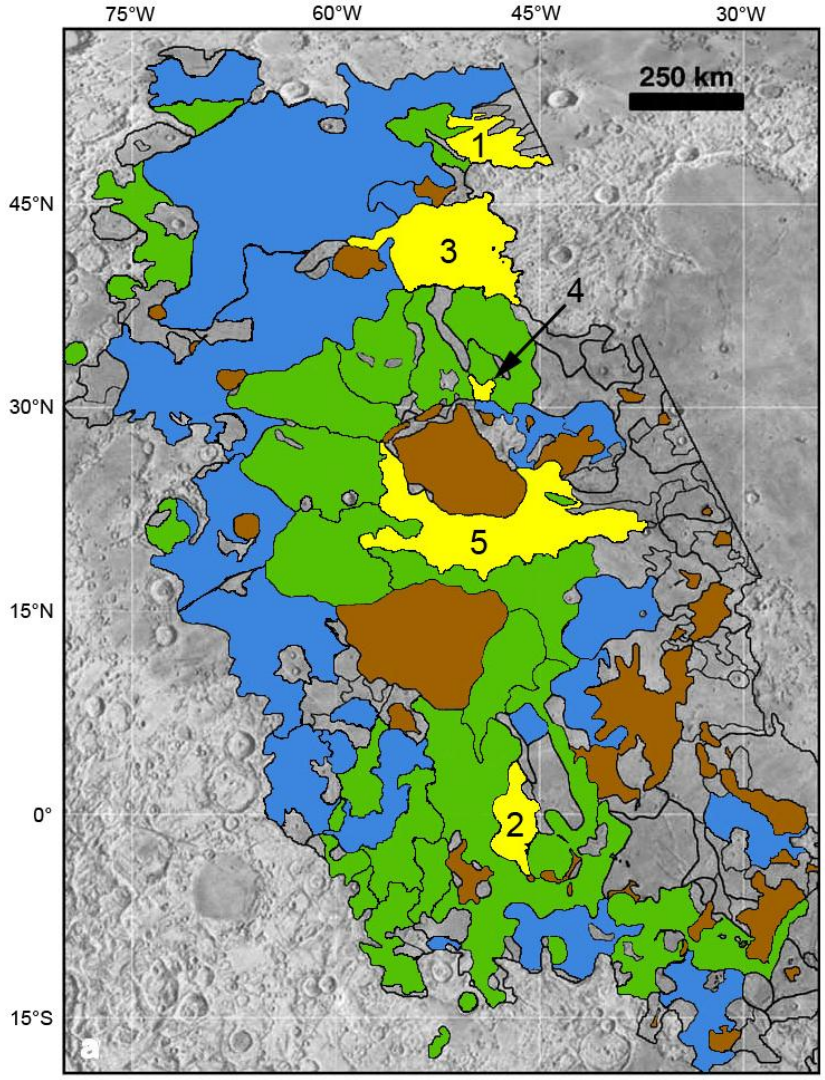

FIGURE 1.34 Map of Oceanus Procellarum outlining individual basalt flows identified by Hiesinger *et al.* (2003). Yellow flows are Copernican, green are Eratosthenian, and blue are Imbrian. Brown areas are nonmare material. Numbers refer to the inferred relative ages of the five Copernican flows (1 being the oldest and 5 the youngest). Flows that have not been filled have not had crater counting conducted on them. (Adapted from Hiesinger *et al.* 2003).

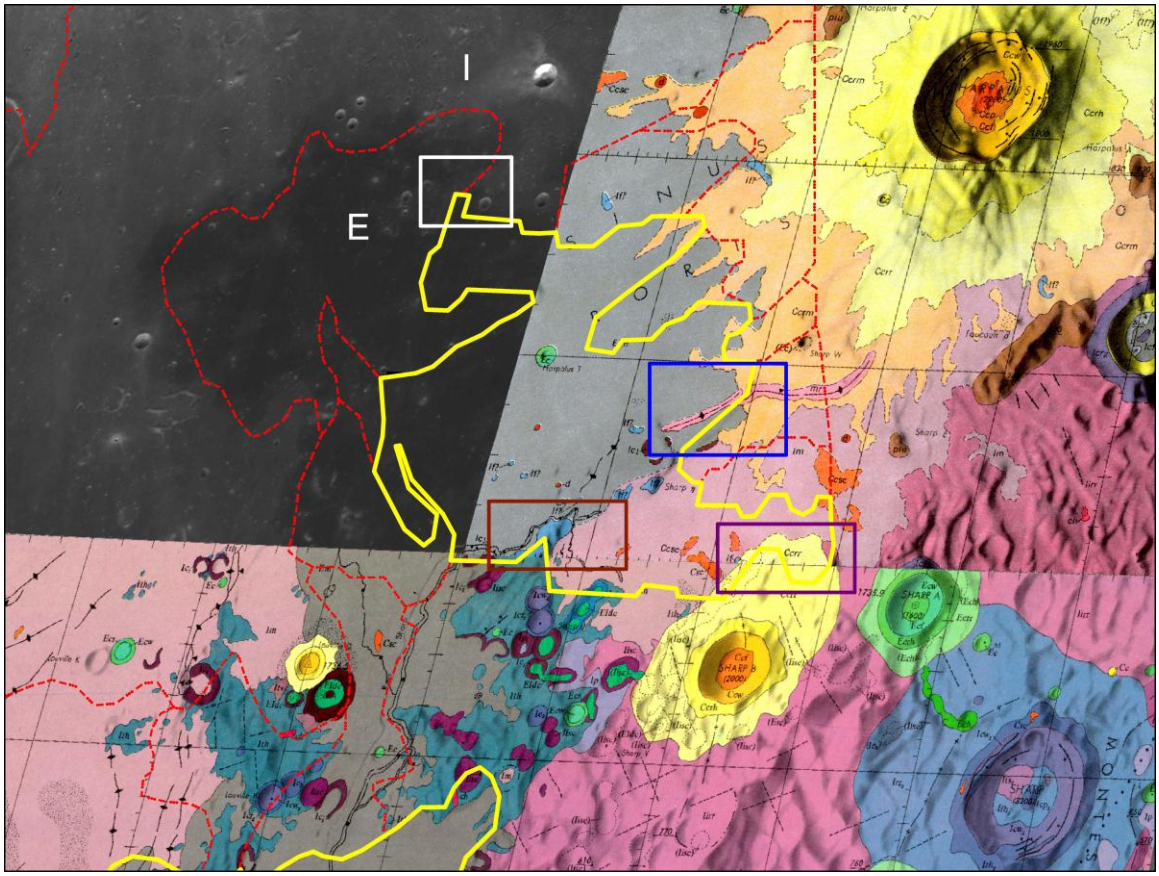

FIGURE 1.35 The oldest Copernican flow identified by Hiesinger *et al.* (2003) is mapped here in yellow on the existing geologic maps of the region (Ulrich, 1969; Scott and Eggleton, 1973). The top of flow 3 (as labeled in Fig. 1.34) can be seen at the bottom of the figure. Surrounding basalt flows are indicated in red. The mapped flows do not match those on the geologic maps because different resolution imagery and data types were used in their identification. Colored boxes indicate sites of scientific interest and are explained in the text. Labels E and I indicate an Eratosthenian and an Imbrian flow respectively.

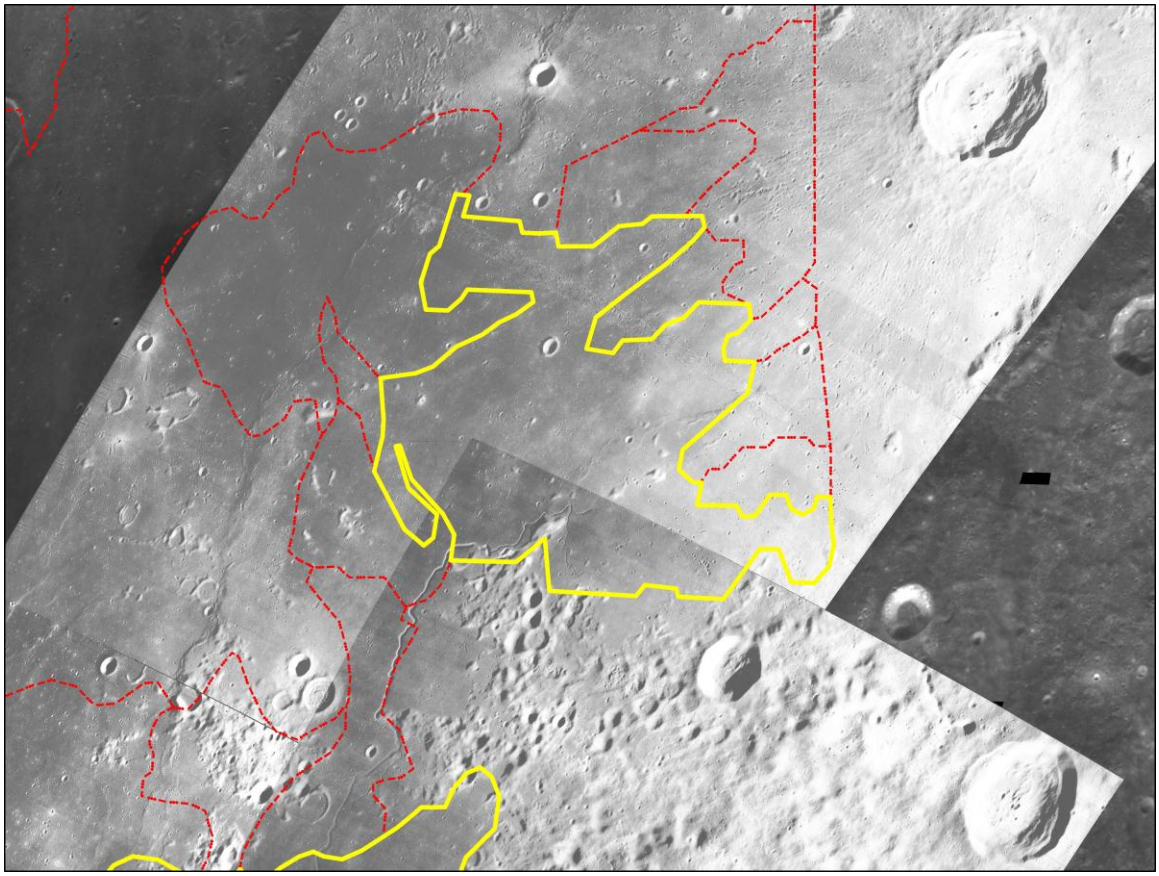

FIGURE 1.36 The oldest Copernican flow identified by Hiesinger *et al*. (2003) is mapped here in yellow on Lunar Orbiter images (LO-IV-4158-H2, LO-IV-4163-H2, LO-IV-4163-H2). The top of flow 3 (as labeled in Fig. 17) can be seen at the bottom of the figure. Surrounding units are indicated in red.

Choosing an exact landing site within this area, with the view to sampling the basalt flow should be carried out on the basis of meeting other scientific goals simultaneously. Figures 1.35 and 1.36 can be used to identify areas of other scientific interest within the region. Colored boxes on Fig. 1.35 indicate examples of such sites:

- White: the Copernican flow at this corner has a contact with two other flows, one that is thought to be Eratosthenian in age and another than is interpreted as Imbrian. By visiting this site and collecting samples from all three flows, a vast range in time should be represented, thus helping to establish a precise chronology (Science Goal 1c).
- Blue: this area contains two different types of rock unit, those of mare basalt material (grey unit labeled *Elm*), and that which contains a mixture of secondary crater (from the Copernican crater Harpalus) and mare material (orange unit labeled *Ccrm*). This area also contains a mare ridge, which is thought to be a structurally controlled fissure volcanic complex whose origin could be investigated by visitation.
- Purple: by visiting this area both crater rim material from the Copernican crater Sharp B (yellow unit labeled *Ccrr*) and the mare basalt material from the area can be sampled (pink unit labeled *Im*).
- Brown: Rima Sharp, an example of a rille is included within this area. Rilles are features whose origins are still not fully understood, and may expose stratigraphy within the mare. The blue geologic unit here is Imbrian ejecta material.

Crater counting and identification

Crater counting should be conducted on surfaces which have either been dated in the past or are dated from future sample return missions. These studies will allow size-frequency distributions for the Copernican period to be improved and thus new chronostratigraphies be applied to other surfaces for relative dating.

Old imagery obtained in the 1960s and 1970s (*i.e.* Lunar Orbiter, Ranger, Apollo) should be systematically compared with newly attained images of the same areas, from current and future lunar missions. The new data must be of equal or better resolution for the purposes of identifying newly formed impact craters on the lunar surface. In the case of higher resolution images, these must be degraded to equal the old images' resolutions to make this a valid undertaking.

Passive seismic network

The Apollo lunar passive seismic network consisted of four stations deployed by the astronauts of Apollo 12, 14, 15 and 16 as part of the ALSEP (Apollo Lunar Seismic Experiments Package). The arrangement of the stations on the near side of the Moon is in approximately an equilateral triangle with 1100 km sides, with two stations 180 km apart at one corner (Fig. 1.37).

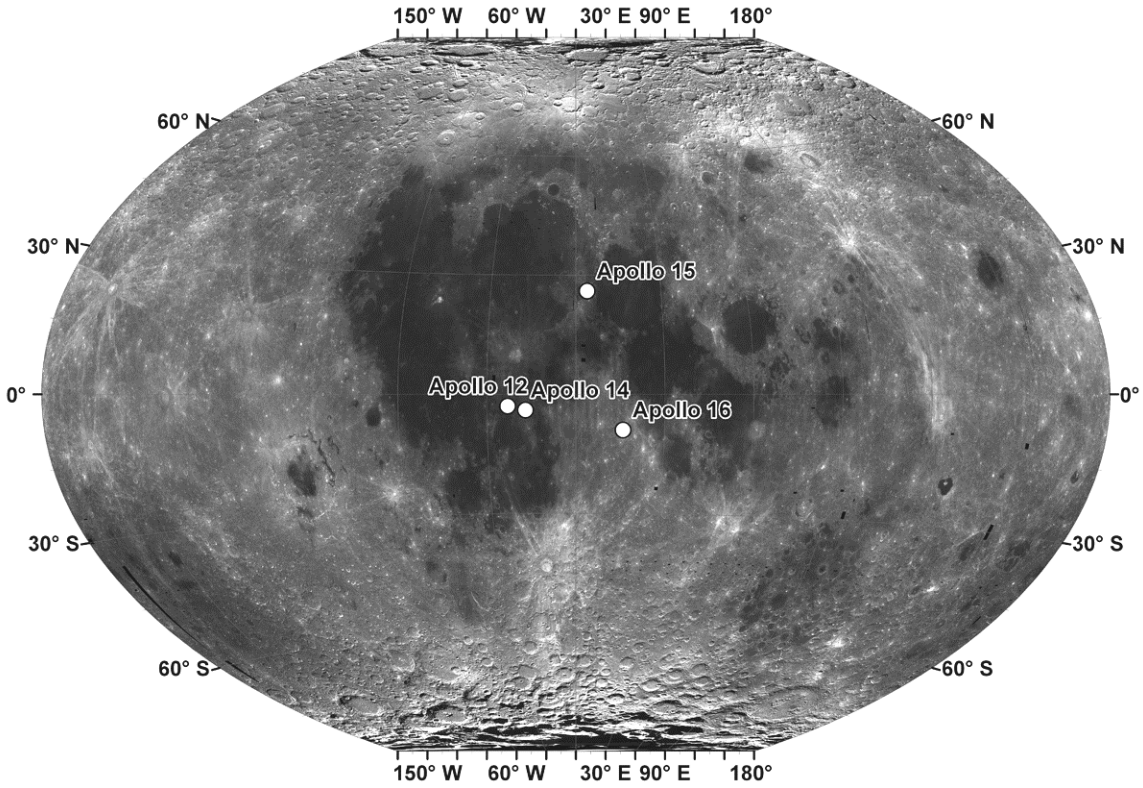

FIGURE 1.37 Map showing the location of the four Apollo passive seismic network stations.

Each station consisted of a set of three long-period (≤ 1 Hz) seismometers sensitive to motion in orthogonal directions and one short-period (> 1 Hz) seismometer sensitive to vertical motion (Fig. 1.38). Two modes of operation of the long-period seismometers were possible: a flat-response mode and a peaked-response mode. Maximum sensitivity was increased (by a factor of 5.6) with the peaked-response mode, but the sensitivity to low-frequency signals was reduced.

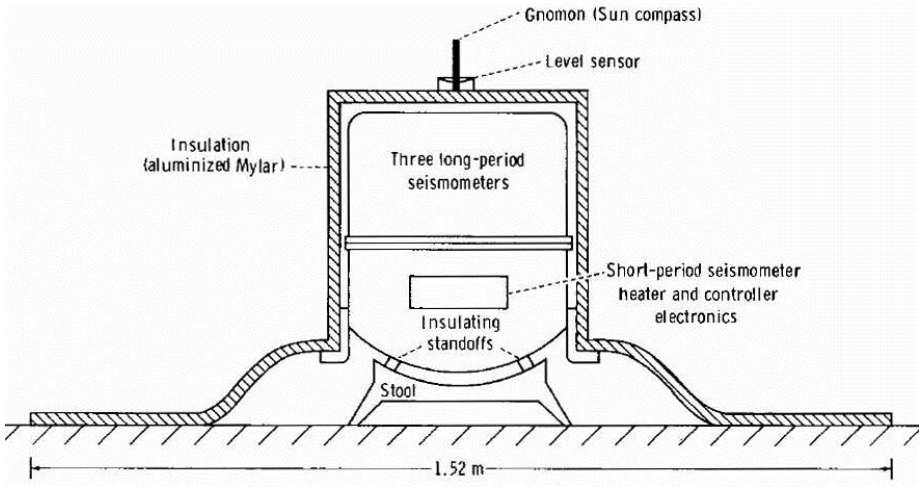

FIGURE 1.38 Schematic diagram of an Apollo passive seismic experiment (Latham *et al.*, 1972)

Meteoroid impact signals were detected by the network. Their signal could be distinguished from moonquake signals by their envelope characteristics: a very weak beginning and a relatively long rise time to the peak amplitude, and the relative weakness of shear waves compared to those from moonquake sources (Latham *et al.*, 1972). Although large impact events are the most energetic of all lunar seismic events, the weak beginning of the signals makes it difficult to locate the impacts by the normal method using P-wave arrival times (Dorman *et al.*, 1978). Each instrument was able to detect ground motions of about 0.05 nm at the peak of its response (Duennebier *et al.*, 1976). During the network's period of operation (1969–1977) a total of 1744 impacts were recorded on the long-period instruments (Nakamura *et al.*, 1982). Oberst and Nakamura (1991) estimate the mass of these meteoroids to have ranged from about 10^{-1} to 10^{3} kg. Rare, larger objects could be detected if they impacted anywhere on the lunar surface, while micrometeoroids could only be detected if they impacted close to a seismic station. These events, from meteoroids smaller than 0.1 kg were too numerous to be counted. Factors other than the mass of the meteoroid affect the seismic signal produced, these include its velocity, density and impact angle.

Several authors have noted that the level of meteoroid impact activity did not occur randomly, but exhibited clustering in time and in the mass distributions (Duennebier *et al.*, 1976; Oberst and Nakamura, 1991). Duennebier *et al.* (1976) concluded that the clustering of meteoroid impacts was not caused by the well-known meteor showers, but occurred in storms lasting from a few days to more than a week and which represented extremely diffuse clouds which had gone previously undetected. Oberst and Nakamura (1991) claim that the clustering of small (<1 kg) and large (>1 kg) meteoroids represents their separate sources: a cometary source for the small population, and near-Earth asteroids or short period comets for the large population.

The results from the Apollo lunar seismic network show that meteoroid impacts can be detected on the lunar surface. The present day impact flux can thus be monitored with the deployment of a new network. The small number of stations, their small areal extent and the short-term nature of the network meant that data were not exhaustive and more seismic information is required. It is highly recommended that a new network be deployed on the lunar surface for the purpose of assessing the recent impact flux. Data quality and scientific output will be improved with more seismic stations and a greater spatial coverage.

A possible New Frontiers Mission was proposed (Neal *et al.*, 2003; Neal, 2005) wherein a new seismic network would be established on the Moon. They envisaged a modest network of eight seismometers (preferably ten) to be deployed around the Moon (including the near side, far side and polar regions) (see Fig. 1.39) and be active for 5 to 7 years.

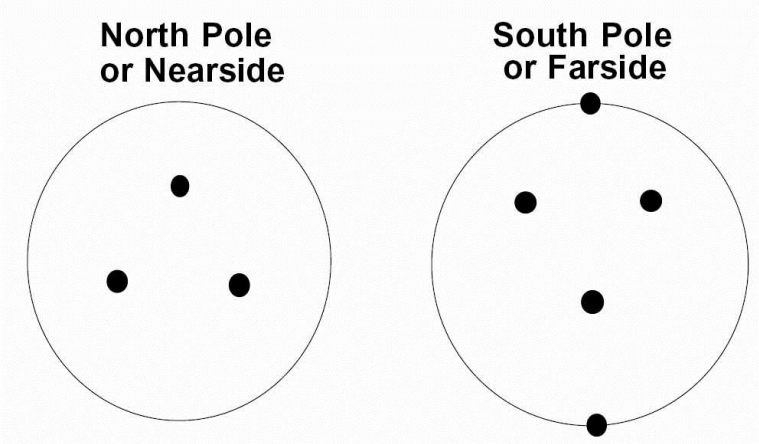

FIGURE 1.39 Schematic seismometer configuration for a lunar seismic network (Neal *et al.*, 2003).

SCIENCE GOAL 1E: STUDY THE ROLE OF SECONDARY IMPACT CRATERS ON CRATER COUNTS

Science Goal 1e is not examined in detail here since its objectives can be attained through orbital imagery and do not require specific landing sites to be achieved.

CONCLUSIONS

To address Science Goal 1a, a representative number of pre-Nectarian, Nectarian, and Imbrian basins need to be sampled and those materials returned to earth for analyses. In some cases, as in the very young Schrödinger and Orientale basins, suitable samples may be exposed over broad areas. In other cases, where basins have been partially filled with volcanic mare, specific sites where younger craters have penetrated the mare and re-exposed the impact melt will need to be targeted.

Because the ejecta blankets of those basins also from stratigraphic horizons that can be used to identify the relative ages of other geologic structures on the Moon, it will be especially productive if the basins were geographically distributed across the lunar surface as well as temporally distributed in time.

The highest priority basin age to determine is that of South Pole-Aitken basin (*i.e.,* Science Goal 1b). Although its ejecta deposits probably contained abundant melt fragments suitable for radiometric dating techniques, they have been severely modified and/or buried by subsequent geologic processes (including younger impact events). For that reason, the best locations for determining the age of the South Pole-Aitken basin are within its interior and, in general, where younger impact events have exposed SPA impact melt-bearing deposits. Good candidates are within an FeO-rich zone in the basin's center and in modestly FeO-enriched sites along the outer margins of the SPA basin (*e.g.*, in the vicinity of Schrödinger basin).

To determine the impact flux after the basin forming epoch, representative craters of Eratosthenian and Copernican age need to be sampled. The most reliable type of sample is from impact melt sheets within the craters or melt-rich deposits in the modification zones or proximal ejecta blankets. The youngest of these basins may have very rough topography and will need to be studied in greater detail to identify specific landing sites. Those types of samples can be used to reconstruct the impact flux over the past half-billion years of lunar history up to and including the present. Details about the most recent impact flux may also be augmented with one or more seismic stations.